

1 A Global Forest Burn Severity Dataset from Landsat Imagery 2 (2003–2016)

3 Kang He^{1,2}, Xinyi Shen³, and Emmanouil N. Anagnostou^{1,2}

4 ¹Department of Civil and Environmental Engineering, University of Connecticut, Storrs, CT 06269, USA

5 ²Eversource Energy Center, University of Connecticut, Storrs, CT 06269, USA

6 ³School of Freshwater Sciences, University of Wisconsin, Milwaukee, Milwaukee, WI 53204, USA

7 Correspondence to: Emmanouil N. Anagnostou (emmanouil.anagnostou@uconn.edu)

8

9 **Abstract:** Forest fires, while destructive and dangerous, are important to the functioning and renewal of ecosystems.
10 Over the past two decades, large-scale, severe forest fires have become more frequent globally, and the risk is expected
11 to increase as fire weather and drought conditions intensify. To improve quantification of the intensity and extent of
12 forest fire damage, we have developed a 30-meter resolution Global Forest Burn Severity (GFBS) ~~database-dataset~~ of
13 ~~information on~~ the degree amounts of biomass ~~that were~~ consumed by fires from 2003 to 2016. To ~~build it~~ develop
14 this dataset, we used the Global Fire Atlas product to determine when and where forest fires occurred during that
15 period and then we overlaid the available Landsat surface reflectance products to obtain pre-fire and post-fire
16 normalized burn ratios (NBRs) for each burned pixel, designating the difference between them as dNBR and the
17 relative difference as RdNBR. ~~W~~First, we compared the GFBS dataset against ~~Using~~ Compared to ~~By comparing with~~
18 the Canada Landsat Burned Severity (CanLaBS) dataset ~~product~~ ~~database~~. ~~we show that found~~ showing that the exhibits
19 showed better agreement than the existing MODIS-based global burn severity dataset (MOSEV) in representing the
20 distribution of forest burn severity to those of CanLaBS over Canada. ~~Second, u~~ Using the in situ burn severity
21 category data available for the 2013 wildfires in southeastern Australia, we demonstrated that GFBS could provide
22 burn severity estimation with clearer differentiation ~~discrepancy between the high-severity class and moderate/and~~
23 low severity classes, while such differentiation among the in situ burn severity classes are not captured ~~obvious in the~~
24 MOSEV product. ~~U~~ Last, u Using the CONUS-wide Composite Burn Index (CBI) as a ground truth, we
25 showed ~~evaluated the performances of GFBS relative to the performances of the existing MODIS-based global burn~~
26 severity dataset (MOSEV). ~~The results showed~~ that dNBR ~~of from~~ GFBS was more strongly correlated with CBI (R^2
27 $r = 0.463$) than dNBR ~~of from~~ MOSEV (R^2 $r = 0.0828$). RdNBR ~~of from~~ GFBS also exhibited better agreement with
28 CBI ($rR^2 = 0.3456$) than RdNBR ~~of from~~ MOSEV ($rR^2 = 0.0420$). ~~At global~~ On a global scale, while the dNBR and
29 RdNBR spatial patterns extracted by GFBS are ~~were~~ similar to those of MOSEV, MOSEV tends ~~tended~~ to provide
30 higher burn severity levels than GFBS. We attribute this difference to variations in reflectance values and the different
31 spatial resolutions of the two satellites.

32

33 1. Introduction

34 In recent years, many regions around the world have experienced an increase in the frequency, intensity, and extent
35 of wildfires (Doerr and Santín, 2016; Shukla et al., 2019; Dupuy et al., 2020). Wildfires are now among the most
36 popular research topics as a result of this rising global concern, which is further heightened by changes expected in
37 fire regimes as a consequence of changes in climate and land use (Moreira et al., 2020). While most wildfires occur
38 in grasslands and savannas (Scholes and Archer, 1997; Abreu et al., 2017), forest fires are more dangerous and
39 destructive and perhaps of greater interest because of their importance to the functioning and renewal of ecosystems
40 (Flannigan et al., 2000; Nasi et al., 2002; Flannigan et al., 2006). Changes brought by the warming climate, which has
41 dried fuels and lengthened fire seasons across the globe (Jolly et al., 2015), are also particularly significant to forested
42 ecosystems with abundant fuels (Kasischke and Turetsky, 2006; Aragão et al., 2018).

43 With the rapid development of remote sensing techniques, more frequent observations from satellites
44 facilitate the monitoring of global fire activities. The valuable information they provide at fine spatial and temporal
45 resolutions can be used to study the number and size distributions of individual fires (Archibald and Roy, 2009;
46 Hantson et al., 2015; Oom et al., 2016), fire shapes (Nogueira et al., 2016; Laurent et al., 2018), and locations of
47 ignition points (Benali et al., 2016; Fusco et al., 2016). Among the most widely accepted techniques are those based
48 on the Moderate Resolution Imaging Spectrometer (MODIS) (Chuvieco et al., 2016), which retrieves information on
49 the entire Earth in 36 spectral bands every one to two days. The MODIS-derived burn area (BA) products are essential
50 for ascertaining the patterns of fire occurrence, extent, propagation (Rodrigues and Febrer, 2018), and frequency
51 (Andela et al., 2019). Based on these products, an essential indicator called “burn severity” has been derived for
52 determining the degree of biomass consumption and the overall impact of fire on ecosystems (Keeley, 2009).

53 Traditionally, burn severity could be quantified from satellite sensors through spectrum information. The
54 changes caused by fire to near-infrared (NIR) and shortwave infrared (SWIR) reflectance are highly sensitive to,
55 respectively, canopy density and moisture content (Chuvieco, 2010). Several burn severity datasets [have been](#)
56 [generated and released](#) based on this method ~~have been generated and released~~. Regionally, the Monitoring Trends in
57 Burn Severity (MTBS) dataset, which includes burn severity assessments for the contiguous United States (CONUS)
58 and provides information on fire perimeters and severity classes, uses satellite data—specifically, Landsat imagery
59 (Eidenshink et al., 2007). Similarly, the Canadian Landsat Burn Severity (CanLaBS) product uses Landsat imagery to
60 assess, and map burn severity at a national scale (Guindon et al., 2021). Globally, MODIS burn SEVerity (MOSEV)
61 has provided monthly burn severity data with global coverage at 500m spatial resolution, based on MODIS Terra and
62 Aqua satellites (Alonso-González and Fernández-García, 2021). ~~However, Despite the satellite those datasets used~~
63 ~~and the target those datasets for, a dataset products~~ for assessing and mapping global forest burn severity based on
64 Landsat [at high spatial resolution](#) (~~(30m resolution)~~ [is are](#) not ~~yet yet~~ available. Such ~~a product~~ [products](#) would support
65 advances in fire management strategies and ecosystem conservation efforts, leading to more resilient and sustainable
66 landscapes.

67 In this paper we describe a new global dataset comprising information on burn severity derived at high spatial
68 resolution [\(30 meter\)](#) from Landsat imagery from the period 2003–2016. This dataset represents a step forward in

69 quantifying and analyzing wildfire impact on forest ecosystems worldwide. We begin with a section detailing the
70 input data and the algorithm ~~we~~ used to process the dataset, as well as the analytical techniques employed. [Section](#)
71 ~~3~~~~The next section~~ presents the characteristics of the dataset and its performance in representing the distribution of
72 forest fires. In the results section, we analyze the advantages and disadvantages of the dataset and set forth its main
73 contributions to forest fire management strategies worldwide. The last section summarizes the primary findings and
74 suggests possible implications of the dataset.

75 **2. Data and Method**

76 Below we delineate the specifics of data input and pre-processing and the analytical techniques we employed to create
77 the dataset. The Global Fire Atlas was the main source of global fire records, ~~which was overlaid~~~~which we overlaid~~
78 with annual land cover types from MCD12Q1 to determine when and where forest fires occurred. We then utilized
79 the reflectance information from Landsat's satellite archives to calculate burn severity indices for the burned forest
80 areas. Finally, we ~~compared GFBS with the CanLaBS dataset available over Canada~~~~Canada,~~ and used the ~~field~~
81 ~~assessed burn severity category data in southeastern Australia and the~~ CONUS-wide Composite Burn Index (CBI) ~~as~~
82 ~~a~~~~the~~ ground truth to evaluate the performances of GFBS relative to that of the existing MODIS-based global burn
83 severity dataset (MOSEV).

84 **2.1. Input data**

85 The input data we used to build the GFBS dataset comprised the fire records available in the Global Fire Atlas for the
86 years 2003–2016 and all Landsat images for the same period.

87 The Global Fire Atlas tracks the daily dynamics of individual fires globally to determine the time and location
88 of ignition, area burned, and duration, as well as daily expansion, fireline length, velocity, and direction of spread. A
89 detailed description of its underlying methodology is provided by Andela et al. (2019).

90 The Terra and Aqua combined Moderate Resolution Imaging Spectroradiometer (MODIS) Land Cover Type
91 (MCD12Q1) Version 6.1 data product provides global land cover types at yearly intervals (Friedl and Sulla-Menashe,
92 2022). With its global coverage and the insights, it offers into the planet's diversity of land cover types, the MCD12Q1
93 dataset is pivotal to various ecological and environmental studies.

94 *Landsat 5,7,8* scene is a 16-day composite image with 7, 8, 11 surface reflectance bands. With its 30 meter
95 resolution and global coverage, it provides a high-quality, atmospherically corrected snapshot of the Earth's surface.
96 Use of the best available observations gathered over the 16-day period ensures the image is as clear and accurate as
97 possible, minimizing issues, such as cloud cover, that can obscure the satellite's view.
98 (<https://developers.google.com/earth-engine/datasets/catalog/landsat>).

99 **2.2. Pre-processing**

100 To pre-process the data, we first imported individual fire polygons from the Global Fire Atlas into the Google Earth
101 Engine (GEE) and then collected the most recent Landsat images based on the tags demarcating the start and end times
102 of each individual fire. We applied a cloud- and snow-masking algorithm to remove any snow, clouds, and their

103 shadows from all imagery based on each sensor’s pixel quality assessment band. By mosaicing the masked images,
104 we created a composite with the smallest possible cloud and shadow extent ([https://developers.google.com/earth-](https://developers.google.com/earth-engine/guides/landsat)
105 [engine/guides/landsat](https://developers.google.com/earth-engine/guides/landsat)).

106 2.3. Algorithm overview

107 ~~We estimated the burn severity indices in two steps, as shown in Figure 1: first, we calculated the normalized burn~~
108 ~~ratios (NBRs) from the mosaiced Landsat composites, and second, we selected the pre- and post-fire NBRs for each~~
109 ~~burned pixel to create burn severity indices—dNBR and RdNBR—based on the differences between the NBRs.~~

110 In the first step, we determined the forest fire polygons using the Global Fire Atlas data associated with the
111 MCD12Q1 land cover data and then utilized reflectance information from Landsat’s satellite archives to obtain the
112 forest fire NBRs from the Landsat composites. Healthy plants absorb most of the visible light (for photosynthesis)
113 while reflecting a large portion of the near-infrared (NIR) light. In contrast, areas that have been burned exhibit low
114 NIR reflectance and high shortwave-infrared (SWIR) reflectance [Key and Benson, 2003; Montero et al., 2023]. This
115 change in spectral properties is due to the loss of vegetation and the exposure of the underlying soil and charred
116 material, which have different reflective characteristics. By computing this ratio for images taken before and after a
117 fire, it's possible to determine the extent and severity of the burn [Cocke et al., 2005; Alcaras et al., 2022].

118 In the second step, we used the pre- and post-fire dates by the Global Fire Atlas data to obtain the
119 corresponding pre- and post-fire NBRs, which allowed us to create the burn severity indices—that is, dNBR and
120 RdNBR—based on the respective differences between them.

121 We took additional steps to validate the performance of the dataset by comparing the burn severity category
122 data over southeastern Australia and CBIs over CONUS with those based on the MOSEV dataset. These steps are
123 detailed in Sections 2.3.1, 2.3.2, and 2.3.3.

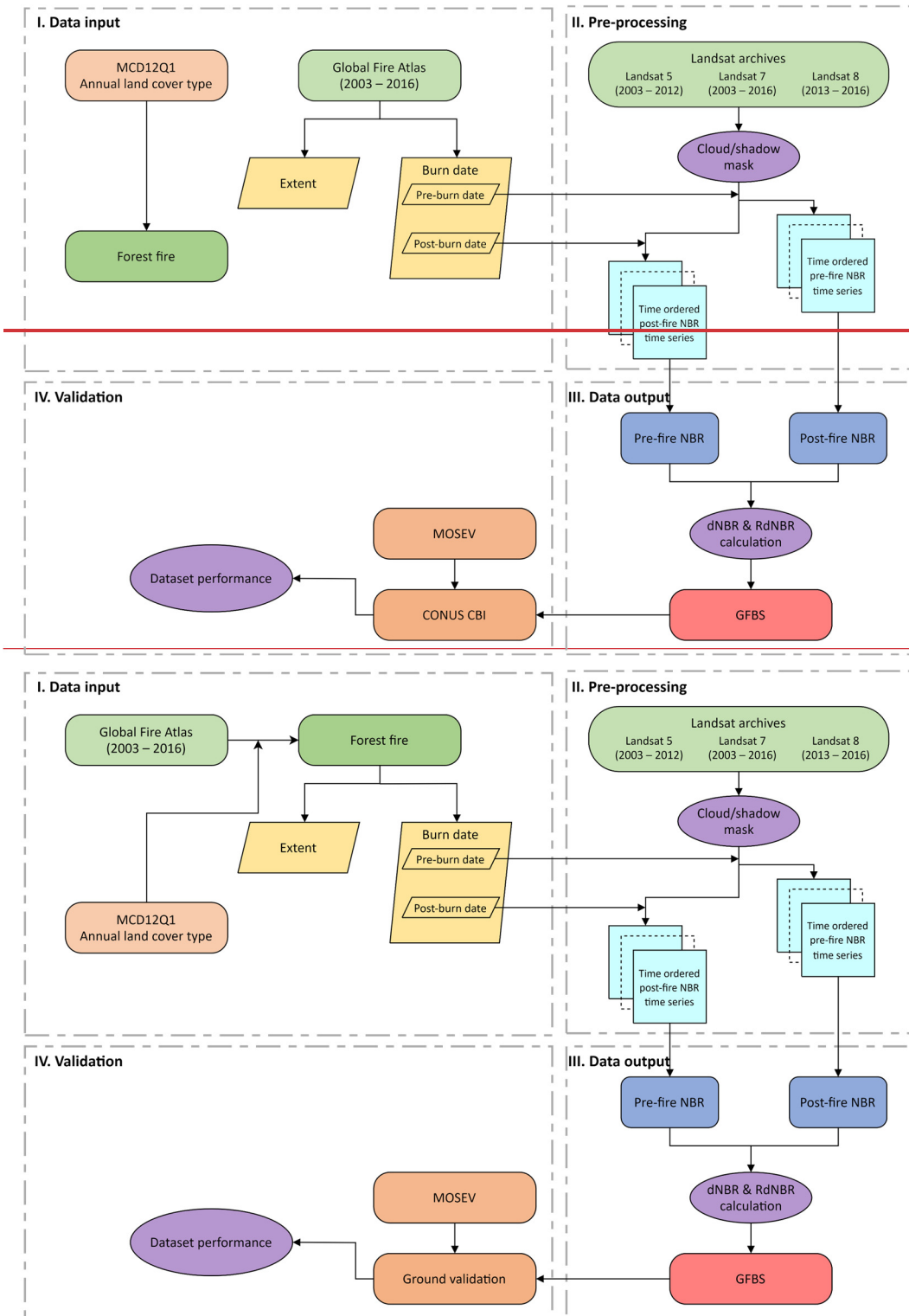


Figure 1. Methodology for building the GFBS database (2003–2016) and validation and comparison with the MOSEV benchmark.

124 2.3.1. Identification of global forest fires

125 To identify global forest fires, we first overlaid the fire polygons from the Global Fire Atlas with MCD12Q1 data
126 from the corresponding year. Based on [Annual International Geosphere-Biosphere Programme \(IGBP\)](#) classifications
127 of land cover, we identified a forest fire polygon within each area where we found forest to be the dominant land cover
128 type within the fire extent—that is, wherever the proportion of burned pixels representing forest, including evergreen
129 needleleaf forests, evergreen broadleaf forests, deciduous needleleaf forests, deciduous broadleaf forests, and mixed
130 forests, was largest relative to the proportion of burned pixels for other land cover types, such as shrublands and
131 grasslands.

132 2.3.2. Estimation of the normalized burn ratio (NBR)

133 We calculated the normalized burn ratio (NBR) spectral index for each Landsat composite. according to the formula
134 in Equation 1 (<https://www.usgs.gov/landsat-missions/landsat-normalized-burn-ratio>):

$$135 \text{NBR} = (\text{NIR} - \text{SWIR}) / (\text{NIR} + \text{SWIR})$$

136 (1)

137 In Landsat series 4 through 7, we collected NIR information from Band 4 and SWIR information from Band
138 7. In Landsat 8, we collected NIR information from Band 5 and SWIR information from Band 7.

139 2.3.3. Estimation of dNBR and RdNBR

140 Having obtained burn area locations and burn dates from the Fire Atlas product, we selected from the Landsat 16-day
141 time series valid pre-fire and post-fire NBR pixels that were, respectively, from the date most closely preceding the
142 start date and the date most closely following the end date of each burned polygon within a three-month time window.

143 The dNBR index, calculated according to Key and Benson (2006) as shown in equation (2), is the reference
144 burn severity spectral index used by the European Forest Fire Information System ([https://effis.jrc.ec.europa.eu/about-](https://effis.jrc.ec.europa.eu/about-effis)
145 [effis](https://effis.jrc.ec.europa.eu/about-effis)) and by the United States' Monitoring Trends in Burn Severity program (<https://www.mtbs.gov>). Larger dNBR
146 values indicate higher burn severity:

$$147 \text{dNBR} = \text{preNBR} - \text{postNBR}$$

148 (2)

149 RdNBR is another burn severity spectral index that is widely used, including by the United States' Monitoring
150 Trends in Burn Severity program (<https://www.mtbs.gov/>, last access:1 May 2021). [The RdNBR normalizes the](#)
151 [dNBR to the square root of pre-fire NBR value, which helps in reducing the variability caused by pre-fire vegetation](#)
152 [conditions and enhances the accuracy in assessing burn severity \[Miller et al., 2009\].](#) As formulated in equation (3)
153 (Miller and Thode, 2007), higher RdNBR values indicate higher burn severity:

$$154 \text{RdNBR} = \text{dNBR} / \sqrt{|\text{preNBR}|}$$

155 (3)

156 2.4. Validation

157 To validate the GFBS database ~~developed in this study~~, we used the 112 ground-verified burn severity category data
158 following the Fire Extent and Severity Mapping (FESM) scheme for the 2013 wildfires over southeastern Australia.
159 The FESM severity classes include unburnt, low severity (burnt understory, unburnt canopy), moderate severity
160 (partial canopy scorch), high severity (complete canopy scorch, partial canopy consumption), and extreme severity
161 (full canopy consumption). Besides FESM, we used the ground-measured CONUS-wide Composite Burn Index (CBI)
162 from 2003 to 2016. CBI was developed by Key and Benson (2006) to assess the aboveground effects of fire on
163 vegetation and soil land use types (i.e., burn severity). It is determined through direct field observations after a fire
164 when assessors visited various sites within the burned area to evaluate the effects of the fire on different components
165 of the ecosystem, such as the degree of charring, percentage of foliage consumed, changes in ground cover, and
166 mortality of plants. The CBI score for each site was calculated by averaging the scores of the different components.
167 This overall score represents the burn severity at a that-specific site. The index ranges continuously from 0-0
168 (unburned) to 3-0 (high severity). These values ~~can behave been compared-related~~ to satellite-derived burn severity
169 ~~data-values to develop through~~ regression equations (<https://burnseverity.cr.usgs.gov/products/cbi>). In this study, we
170 used all available CBI values over CONUS to establish ~~the regression-relationships~~ between CBI and the dNBR and
171 RdNBR values of the GFBS ~~and MOSEV database datasets~~. We ~~applied-used~~ the Pearson correlation coefficient and
172 biaseoefficient of determination as metrics to evaluate the performance of ~~GFBS the two datasets relative to the~~
173 ~~corresponding performance of the MOSEV database, which is currently used to evaluate global burn severity.~~ Figure
174 2 (a) shows the locations of the 112 ground-verified burn severity sites for the 2013 wildfires over southeastern
175 Australia. Figure 2 (b) shows the locations of available CBI observations s-over CONUS from for the period from 2003
176 to 2016. Of the 1,315 ground-surveyed CBI reports for forest fires during that time, most came from western states,
177 such as Arizona, Colorado, and Oregon, where forest fires are more frequent and severe. Fewer CBI records are
178 available in eastern states, such as Florida and Georgia.

179 ~~In addition to validation against in situ data., we also compared the fire severity magnitudes of GFBS with the~~
180 ~~CanLaBS dataset available over Canada. CanLaBS provides burn severity information for burned areas identified~~
181 ~~from the Canada Landsat Disturbance product at the level of individual 30m resolution pixels. The dataset was derived~~
182 ~~developed from Landsat imagery and uses values of pre fire to post fire differences in dNBRs for nearly 60 million~~
183 ~~hectares of burned areas across Canada's forests from 1985 to 2015. [Guindon et al., 2017; Guindon et al., 2018].~~

184 ~~Figure 2 (a) shows the locations of the 112 ground-verified burn severity sites for 2013 wildfires over southeastern~~
185 ~~Australia. Figure 2 (b) shows the locations of available CBIs over CONUS from 2003 to 2016. Of the 1,315 ground-~~
186 ~~surveyed CBI reports for forest fires during that time, most came from western states, such as Arizona, Colorado, and~~
187 ~~Oregon, where forest fires are more frequent and severe. Fewer CBI records are available in eastern states, such as~~
188 ~~Florida and Georgia.~~

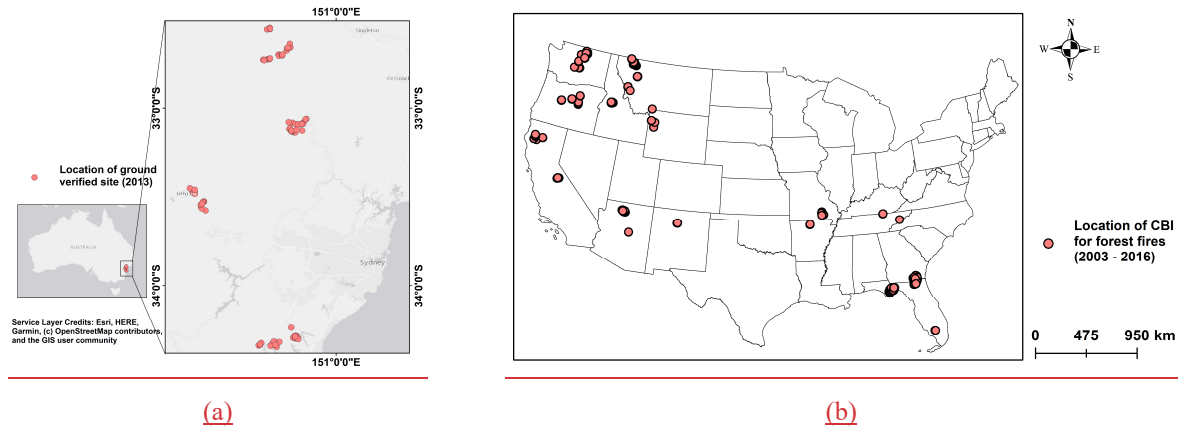


Figure 2. Locations of (a) ground verification burn severity sites over southeastern Australia and (b) forest fire CBIs over CONUS.

189
190
191
192
193
194
195

[In addition to validation against in-situ data., we also compared the fire severity magnitudes of GFBS with the CanLaBS dataset available over Canada. CanLaBS ~~provides~~provides burn severity information for burned areas identified from the Canada Landsat Disturbance product at the level of individual 30m resolution pixels. The dataset was derived from Landsat imagery and uses values of pre-fire to post-fire differences in dNBRs for nearly 60 million hectares of burned areas across Canada's forests from 1985 to 2015. \[Guindon et al., 2017; Guindon et al., 2018\].](#)

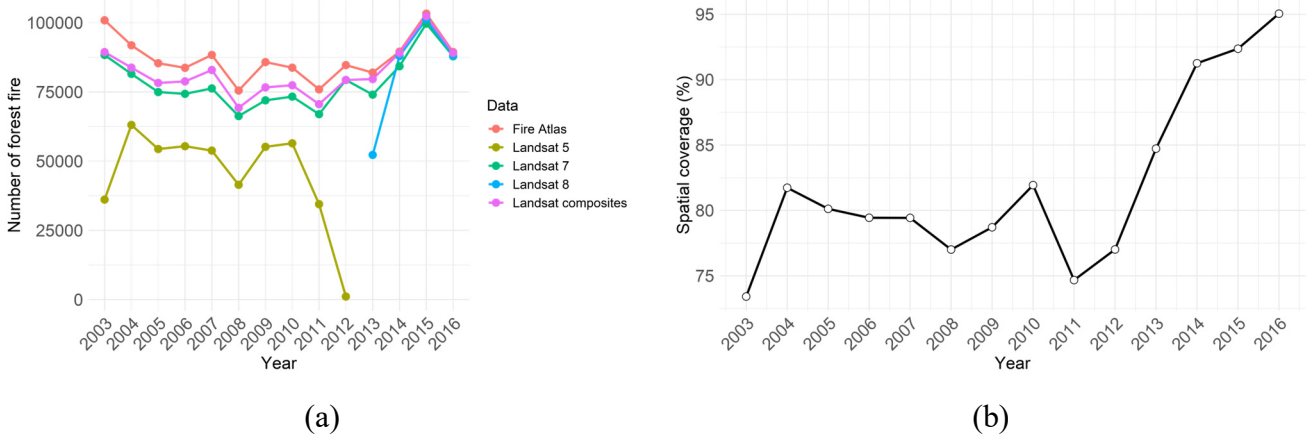
196 3. Results

197 3.1. ~~Forest fire coverage of Landsat composites.~~Landsat mosaiced composites

198 Figure 2-3 (a) shows the number of forest fire polygons globally between 2003 and 2016, representing individual fire events, from the Global Fire Atlas dataset. Approximately 80,000 forest fire events occur in the world each year on average, ~~with where~~ more than 90,000 ~~happening-happened~~ in 2004 and more than 100,000 in 2003 and 2015, respectively. Figure 2-3 (a) ~~also~~ displays the availability of Landsat imagery covering the burn area where individual forest fires happened worldwide. From 2003 to 2012, Landsat 5 could provide images covering ~~only-between~~ 35% ~~to~~ ~~and~~ 68% of the recorded forest fire events in the Global Fire Atlas, while Landsat 7 images ~~could-covered~~ 83% to 93% ~~of the Global Fire Atlas events~~. From 2013 to 2016, Landsat 7 images covered ~~about-between~~ 90% ~~to-and~~ 98% of the fire events, while Landsat 8 images covered more than 97%. The Landsat composites combining all available Landsat 5 and Landsat 7 images from 2003 to 2012 and Landsat 7 and Landsat 8 images from 2013 to 2016 significantly increased the number of forest fires shown by Landsat images, with coverage of the fire events ranging from 88% to 99%. Figure 2-3 (b) shows the distribution of the spatial coverage of cloud-free Landsat composites for individual fires from the Fire Atlas. We used a cloud and shadow removal algorithm to eliminate invalid poor-quality pixels from recorded forest fires, resulting in a line chart showing the distribution of the percentages of valid pixels to

209
210

211 the total burn pixels in each year. Overall, the spatial coverage was above 72%, and the coverage has been above 85%
 212 since 2013, when Landsat 8 was launched.



213
 214 **Figure 23. (a) Numbers of individual fires from the Fire Atlas and available Landsat imagery; (b) Spatial coverage**
 215 **of cloud-free Landsat composites for individual fires ~~from~~ reported in the Fire Atlas.**

213

214 Figure 4 shows displays the data process for a single post-NBR Landsat composite for the fire event that
 215 ended on 17 September 2015 in north Washington. The first prior image for NBR calculation ~~was~~ on 20 September
 216 2015 from Landsat 8 (as image 1). The cloud and shadows are removed in image 1 after applying the cloud/shadow
 217 mask. The next available image on 21 September 2015 from Landsat 7 (as image 2) ~~was~~ then used to fill those gaps
 218 in image 1 and obtain a new Landsat composite (phase 1). The third available image on 29 September 2015 from
 219 Landsat 8 (as image 3), image on 15 October 2015 if needed, ~~was is~~ adopted sequentially to fill the un-scanned gap
 220 pixels in phase 1 and generate the final post NBR image for this event. The process for pre-NBR image calculation is
 221 the same but in a reversed time-order from the start time of the fire event.

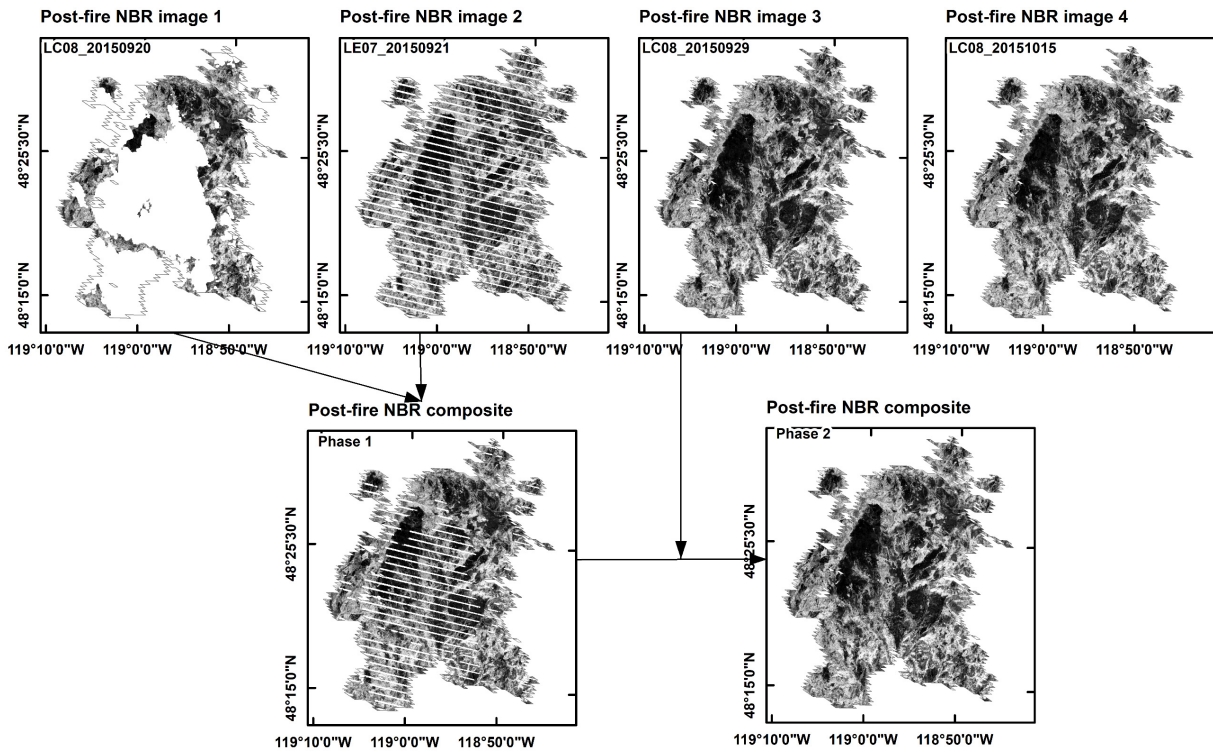


Figure 4. NBR image process for Landsat composite, for the fire event ended on 17 September 2015 in north Washington.

222

223 The scatterplot in Figure 5 (a) shows the NBR values of the overlapping pixels in image 1 and image 2, with
 224 the associated distributions of NBR for the fire event. It is noted that NBR values in images 1 and 2 show high
 225 correlation (with $r = 0.96$), relatively low bias ($= -23.81\%$) and similar probability densities, even though they
 226 are though are derived from two different Landsat images (Landsat 8 and Landsat 7). The scatterplot in Figure 5 (b)
 227 shows the NBR values of overlapping pixels in image 1 and image 3, with the associated distribution of NBR for the
 228 fire event. Similarly, NBR values in image 1 and image 3 have high correlation (with $r = 0.96$) and low bias ($=$
 229 12.30 %) and similar probability densities, even though they are density though are derived from different times (with
 230 a 9 -days apart) interval. The results indicate that the cloud-free NBR composite mosaicking of all available Landsat
 231 images has reasonable accuracy with high spatial and temporal consistency.

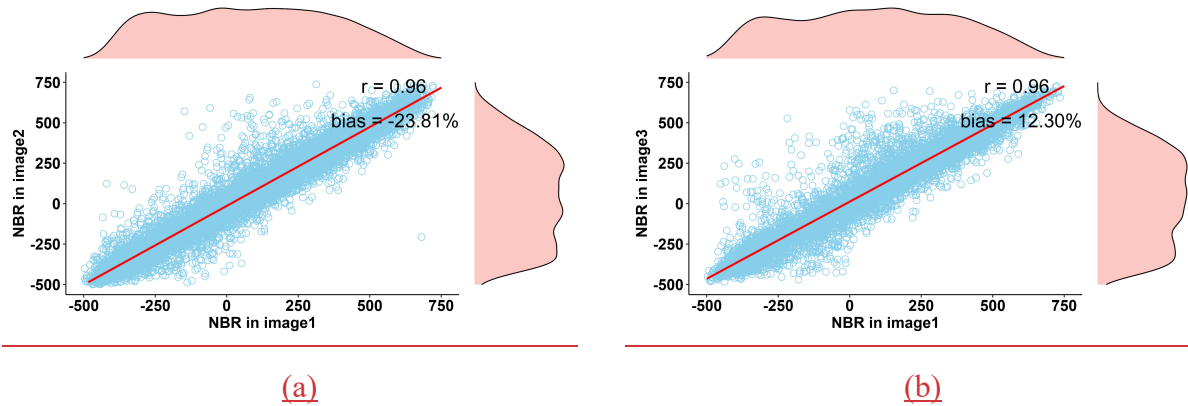


Figure 5. Scatterplots of overlapped pixel values in (a) image 1 and image 2; (b) image 1 and image 3.

232
233
234
235
236
237
238
239
240
241

3.2 Comparison between GFBS and CanLaBS over Canada

In this section we describe the We-comparison of edrespectively the fire severity maps of GFBS and MOSEV datasets to the ones from the CanLaBS dataset over Canada for an overlapped period from 2003 to 2015. Figure 6 shows the number and the trend of forest fires over Canada from 2003 to 2015, by CanLaBS data and GFBS products, while the vertical bar represents the number of forest fires recorded by both CanLaBS and GFBS each year. Due to the different sources and algorithms to map the burn area, the number of forest fires depicted by CanLaBS is larger than those by GFBS each year. It is noted Nevertheless, it is noted that GFBS agrees with CanLaBS in terms of the variations of forest fire activities, such as the intense forest fires in 2004 and 2015 and the relatively low number of forest fires in 2007 and 2008.

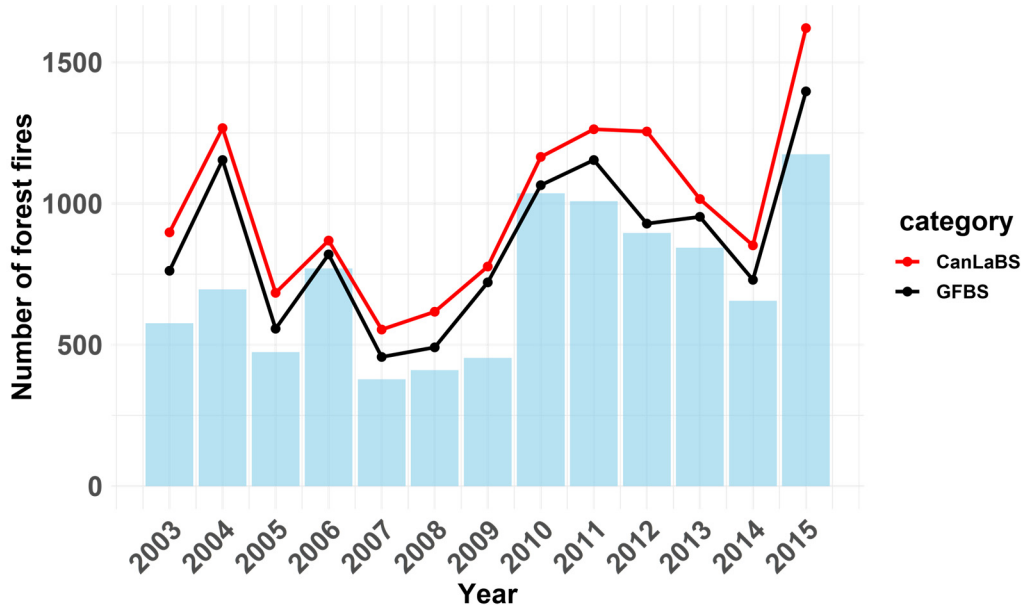
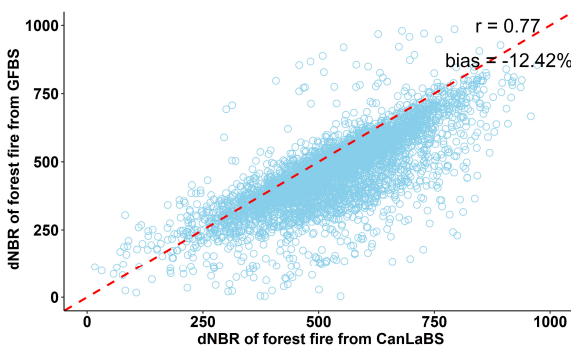


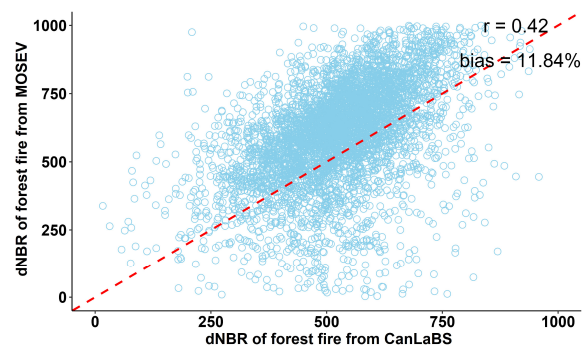
Figure 6. Number of forest fires by CanLaBS and GFBS dataset. Vertical bars show the number of overlapping forest fires.

242

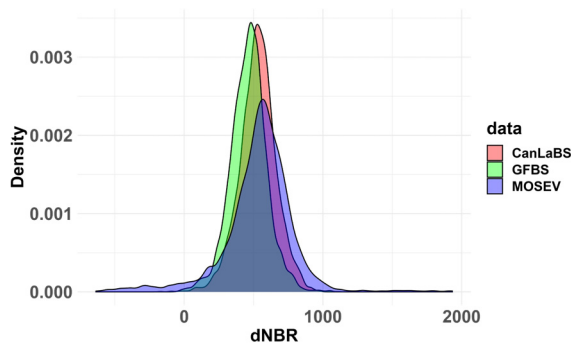
243 Figure 7 illustrate the scatterplots of dNBR of forest fires from CanLaBS against those from GFBS (panel a)
244 and MOSEV (panel b), for the period from 2003 to 2015. Consistent to the results shown in Figure 6, dNBR from
245 GFBS shows ~~strong~~ ~~stronger~~ correlation with the dNBR from CanLaBS with r being 0.77 and a slightly
246 ~~underestimation of~~ ~~underestimate~~ the overall dNBR for forest fires (~~with bias = being~~ -12.42%). On the other hand,
247 ~~While dNBR from MOSEV exhibited low correlation with the dNBR from CanLaBS performed worse when~~
248 ~~compared to dNBR from CanLaBS (ith r = being~~ 0.42) and slight overestimation (bias = being -11.84 %). Figure 7 (c)
249 displays the probability density function (PDF) plots of CanLaBS dNBR, GFBS dNBR and MOSEV dNBR. It is noted
250 ~~the close that~~ PDFs of GFBS dNBR ~~and is closer to the PDF of~~ CanLaBS dNBR, though the mode of GFBS
251 ~~distribution is at slightly lower dNBR value relative to the CanLaBS distribution.~~ On the other hand, ~~the~~ distribution
252 of MOSEV dNBR significantly deviates from CanLaBS dNBR, ~~having and has a~~ lower peak and larger tails.



(a)



(b)



(c)

Figure 7. Scatterplots of dNBR from CanLaBS against those from (a) GFBS and (b) MOSEV; (c) density plot of dNBR from CanLaBS, GFBS and MOSEV, for forest fires from 2003 to 2015 over Canada.

253

254 Last Figure 8 presents the boxplots of distributions of dNBR from CanLaBS, GFBS and MOSEV separate
 255 by year for each year from. Consistent to the previous results, GFBS compares well with CanLaBS in terms of the
 256 dNBR distribution of dNBR for annual forest fires and as well as the variations of dNBR over time, even though it
 257 provides slightly lower dNBR values compared to CanLaBS. On the other hand, MOSEV compared poorly with
 258 CanLaBS annual dNBR in terms of the distributions, of dNBR exhibiting overall larger dNBR values and larger
 259 anomalies over time.

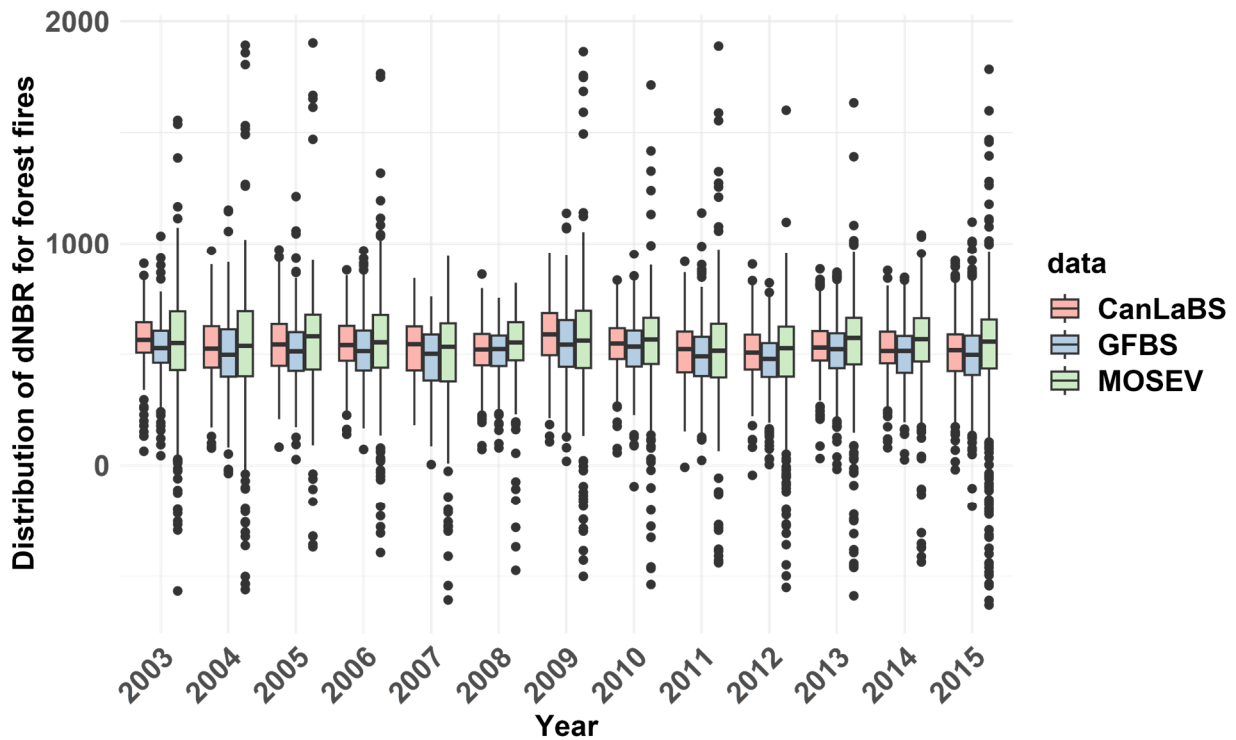
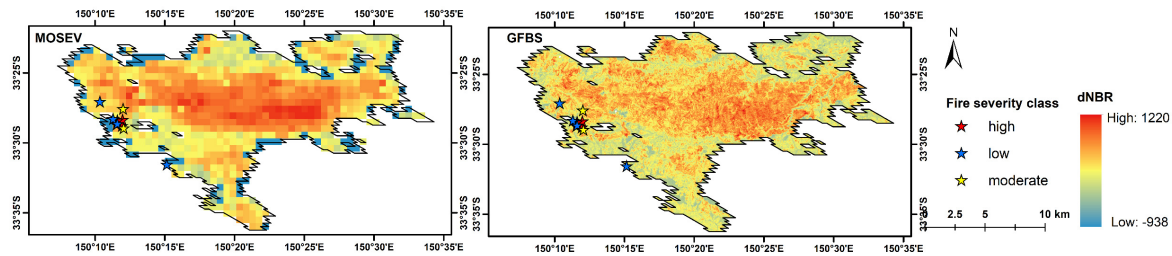


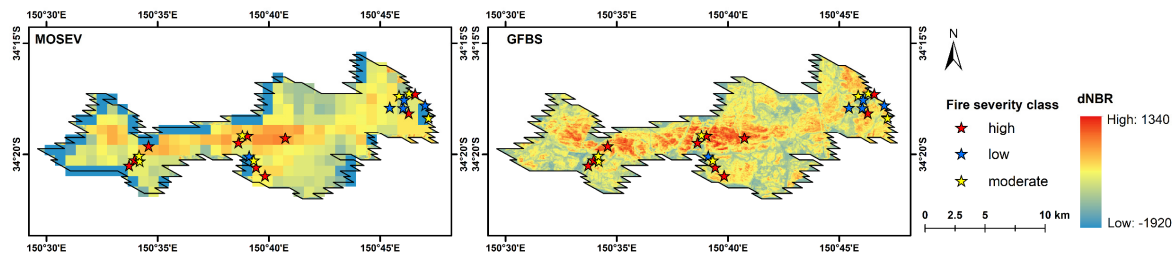
Figure 8. Boxplots of annual distributions of dNBR values from CanLaBS, GFBS and MOSEV for forest fires over Canada from 2003 to 2015.

260 **3.3. Validation against in situ fire severity category over southeastern Australia**

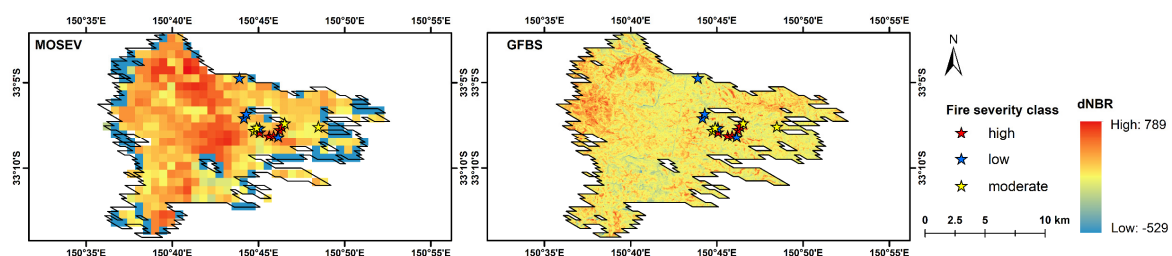
261 Using as the ground truth the in-situ ground-verified burn severity categorizations from the 2013 wildfires over
 262 southeastern Australia, we evaluate the performance of GFBS and MOSEV datasets in the 2013 wildfires over
 263 southeastern Australia. Figure 9 (a), (b) and (c) display the spatial patterns of GFBS dNBR and MOSEV dNBR for
 264 wildfires that happened on October 15 2013, October 17 2013 and October 21 2013, respectively, in southeastern
 265 Australia, where relatively dense in situ burn severity categorization data are available. It is noted that GFBS dNBR
 266 shows similar spatial patterns to the MOSEV dNBR in the events on October 15 2013 and October 17 2013, both
 267 showing significant fire centers where high dNBR are found. For the October 21 2013 event, however, the dNBR map
 268 from MOSEV shows a larger high burn severity area than GFBS.



(a)



(b)



(c)

Figure 9. Spatial patterns of dNBR for wildfires on (a) October 15 2023, (b) October 17 2023 and (c) October 21 2023, in southeastern Australia, derived from the GFBS and MOSEV datasets.

269

270 The boxplots in Figure 10 (a), (b) and (c) display the corresponding distributions of dNBR from GFBS and
 271 MOSEV at different observed severity classes in the events on October 15 2023, October 17 2023 and October 21
 272 2023, respectively. The severity classes, e.g. low, moderate and high, are categorized from the field assessed sites in
 273 the corresponding fire events. For the event on October 15 2023, dNBR from GFBS shows significant difference
 274 between the moderate/high and low severity class, and no difference between high and moderate severity class. The
 275 dNBR from MOSEV, however, presents lower dNBR at high severity class than those at moderate and low severity
 276 class. For the event on October 17 2023, both GFBS and MOSEV show significant discrepancies on dNBR between
 277 high and moderate/low severity class. For the event on October 21 2023, GFBS could clearly differentiate among
 278 high, moderate and low severity classes in terms of dNBR values, while MOSEV presents the lowest dNBR
 279 values at the moderate severity class, while exhibits small differences in dNBR values between the low and high
 280 severity classes. Figure 10 (d) shows the overall performances of dNBR from GFBS and MOSEV for the different

281 severity classes, combining all 112 ground verification sites. More significant differences are shown in the GFBS
 282 dNBR boxplots between high, moderate and low severity classes than those from MOSEV, indicating a better skill of
 283 GFBS to distinguish between forest fires of different severity levels.

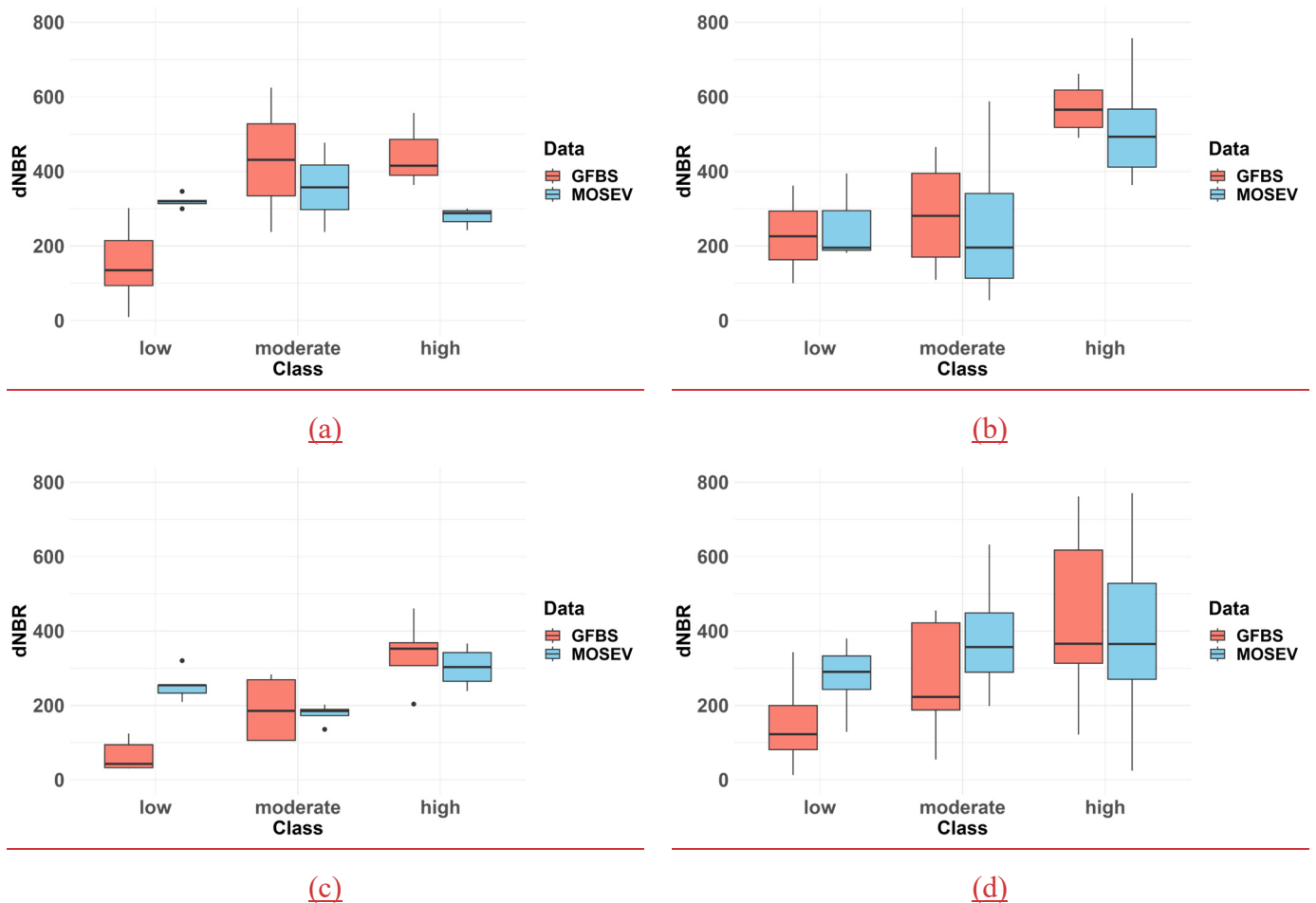
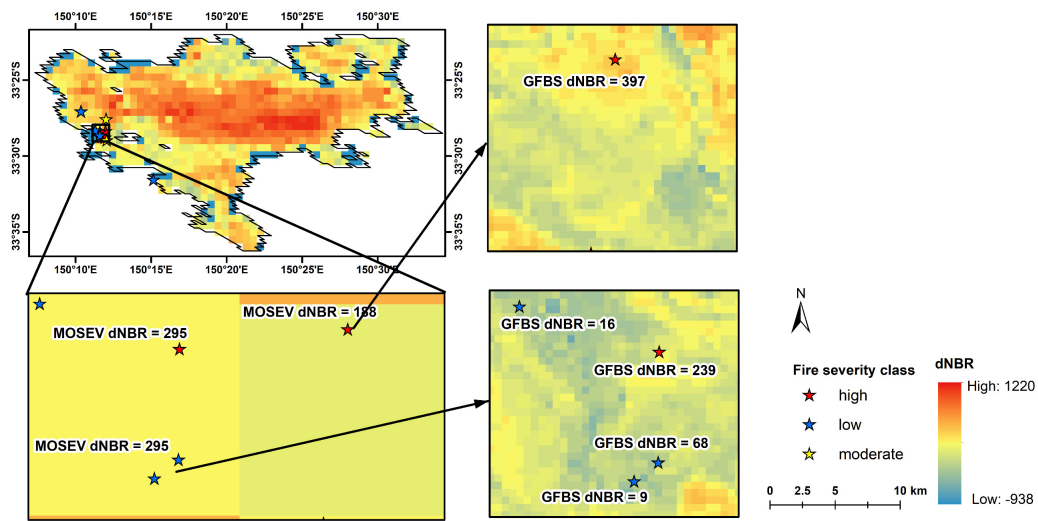


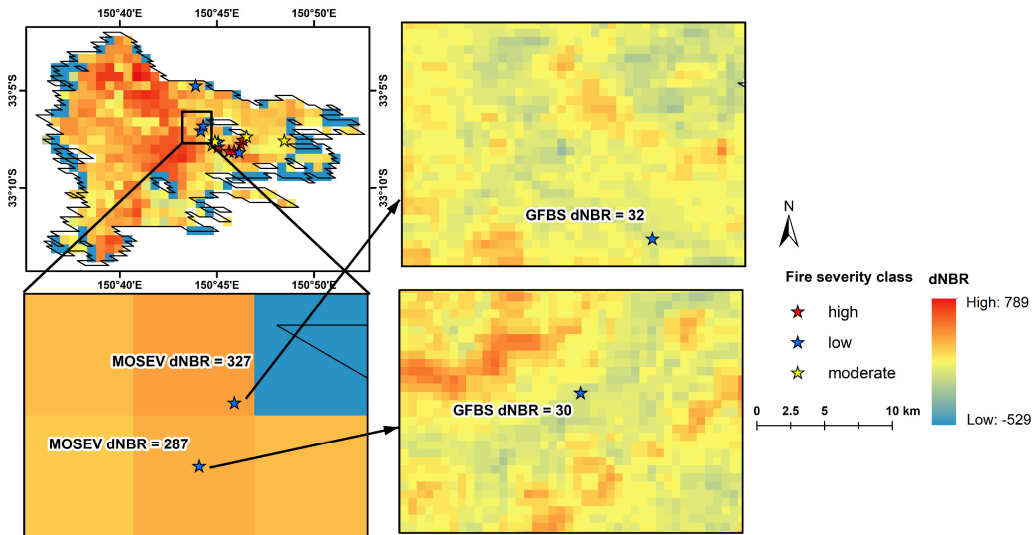
Figure 10. Boxplots of distributions of dNBR at different burn severity classes from the in situ data category classified from the in situ by ground-verified data for (a) event on October 15 2023; (b) event on October 17 2023; (c) event on October 21 2023; and (d) combining events involve all events with in situ data ground-validation.

284
 285 As mentioned above, MOSEV gave relatively small dNBR values in the event on October 15 2023, where
 286 burn severity is classified from in situ measurement as high. Figure 11 (a) displays the location of the ground
 287 verification sites with the corresponding burn severity class and associated dNBR values from MOSEV and GFBS. It
 288 is noted that within one MOSEV grid cell (500 meter) four 4-ground verification sites are located. The dNBR value
 289 from MOSEV is 295 for all four sites, while three of the sites are classified as low and only one site is classified as
 290 high severity. On the other hand, at GFBS resolution (30 meter), we can note significant spatial variation in
 291 dNBR shown found, with GFBS dNBR being 239 for on the 1-site classified as high and 9, 16 and 68 for the three sites
 292 classified as low severity. In a surrounding MOSEV pixel we note a site classified as 1-high severity is located site is

293 located, but dNBR from MOSEV is 188 while dNBR from GFBS is 397. In the event on October 21 2023, we found
 294 that MOSEV gave relatively high dNBR values at ground verification sites that are classified as low severity. Figure
 295 11 (b) shows the locations of ground verification sites with corresponding classified burn severity and associated
 296 dNBR values from MOSEV and GFBS. In the two adjacent MOSEV grids, the dNBR values from MOSEV are 287
 297 and 327 respectively where both sites are classified as low severity. At GFBS resolution more significant changes
 298 between high and low dNBR are found within the same MOSEV grid, resulting in dNBR values of 30 and 32 for the
 299 ground verification sites classified as low severity. The results demonstrate the significance superiority of GFBS high
 300 resolution data in representing the small-scale variations of dNBR and providing more granular and reliable dNBR
 301 estimations, due to the improved spatial resolution.



(a)



(b)

Figure 11. The location of ground verification sites with classified burn severity classes overlaid by and associated dNBR values from GFBS and MOSEV for the fire event of (a) October 15 2023 and (b) October 21 2023.

302

303 **3.24. Validation against CBI over CONUS**

304 Figure 3 shows the spatial locations of available CBIs over CONUS from 2003 to 2016. Of the 1,315 ground surveyed
 305 CBI reports for forest fires during that time, most came from western states, such as Arizona, Colorado, and Oregon,

306 where forest fires are more frequent and severe. Fewer CBI records are available in eastern states, such as Florida and
307 Georgia.

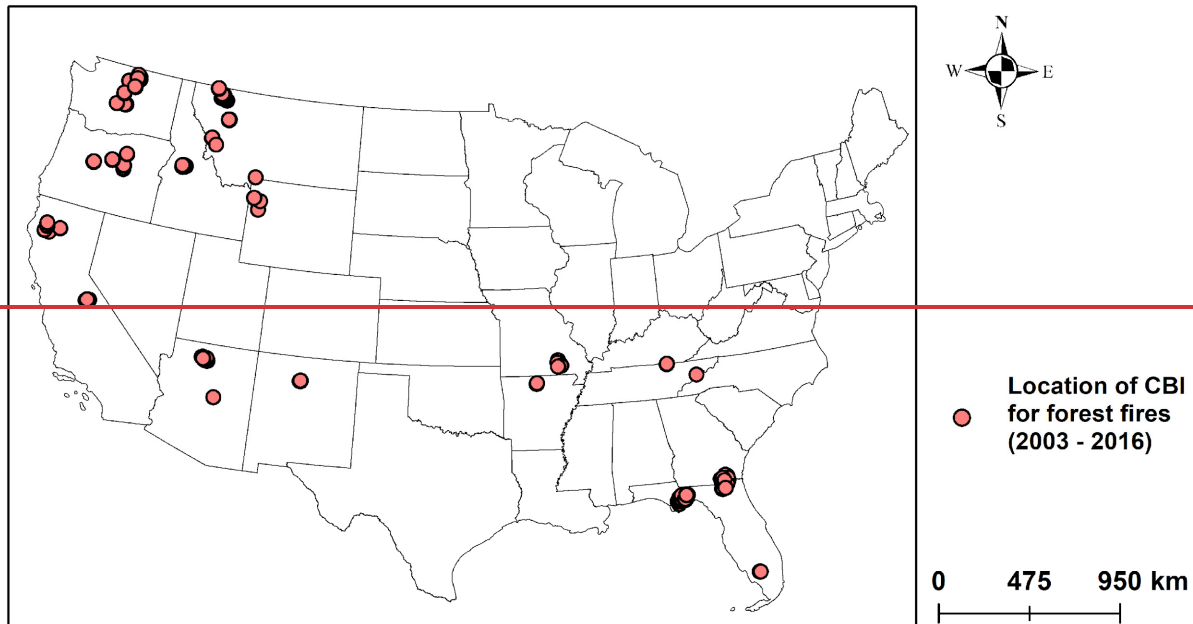
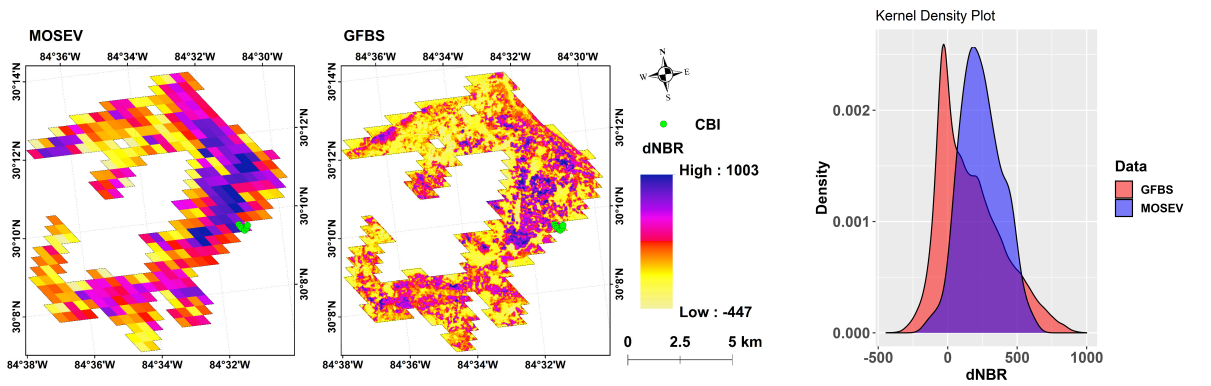


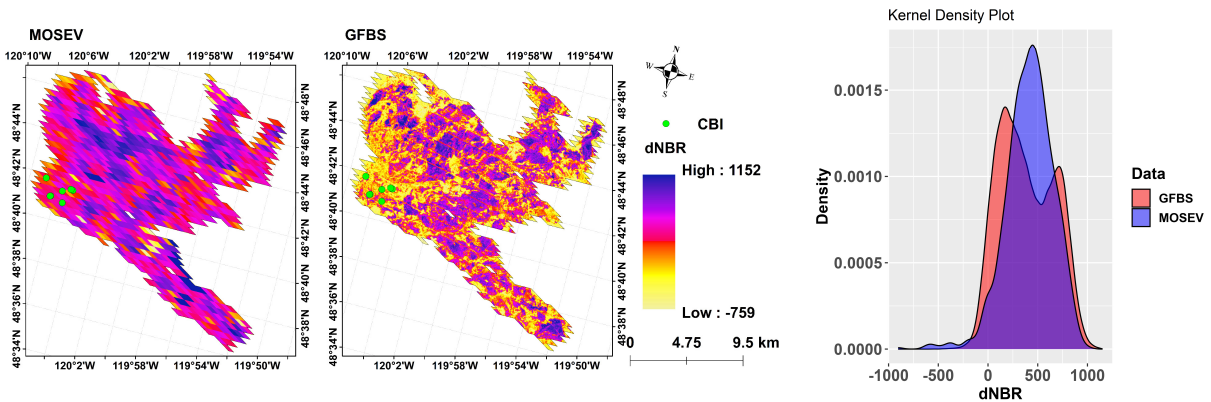
Figure 3. Spatial locations of forest fire CBIs over CONUS.

308
309 Figure 4-12 (a), (b), (c) and (d) shows the spatial patterns of dNBR derived from GFBS and MOSEV over CONUS
310 for the forest fires with the largest burn areas (referred to as annual maximum forest fire hereafter) in 2004, 2006,
311 2007, and 2013 respectively for which CBI records are available. The figures present the associated probability density
312 functions (PDFs) of dNBR values from GFBS and MOSEV, along with spatial distribution maps of dNBR. The
313 similarity in spatial patterns between GFBS burn severity and MOSEV burn severity is noted in these plots obvious.
314 Significant differences occur, however, between GFBS-dNBR from and GFBS and MOSEV-dNBR. We found that,
315 when we relied on MODIS products, MOSEV dNBR tended to underestimate the high severity and overestimate the
316 low severity of the annual maximum forest fire in 2004, compared with GFBS dNBR. Specifically, MOSEV tends to
317 providetends provide overall larger dNBR values, but where dNBR from GFBS is relatively high MOSEV dNBR
318 values are relatively lower where dNBR from GFBS is relatively low and smaller and provide smaller dNBR where
319 dNBR from GFBS is relatively high. This difference could also be inferred from the PDFs of dNBR from GFBS and
320 MOSEV, where MOSEV-dNBR from MOSEV distributed more on the mean value of dNBR of around 300, while
321 GFBS-dNBR from GFBS is bi-modal with peaks on both low and high values distributed more on the extreme low and
322 high values. For the annual maximum forest fire in 2007, especially, MOSEV-dNBR MOSEV greatly
323 generally overestimated showed more extensive areas with high the severity dNBR values levels compared to GFBS
324 dNBR, a difference that was also reflected-revealed in the large deviation of mean dNBR values in the PDFs of dNBR
325 for from the GFBS (mean dNBR around 100) and MOSEV (mean dNBR around 500) datasets.

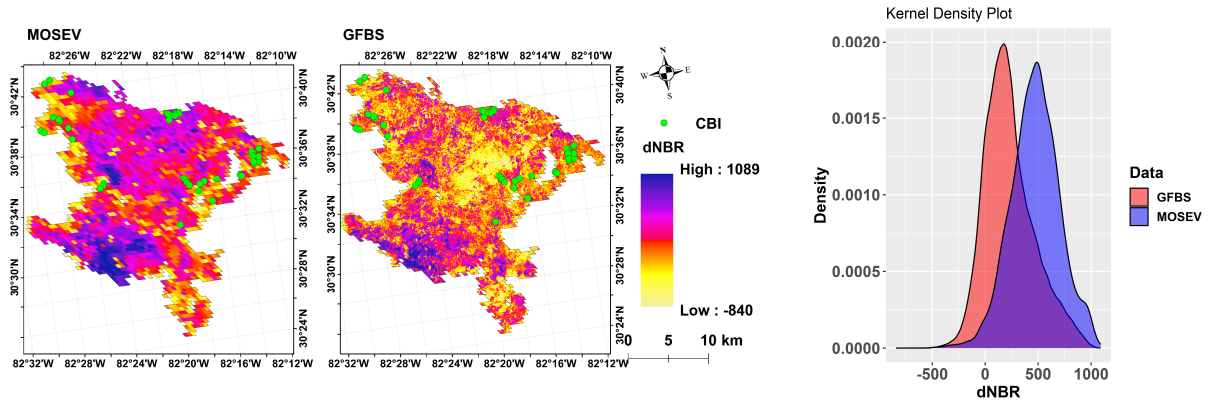
326 The density plot of dNBR in Figure 4-12 also clearly shows the bi-modal two peaks distribution for GFBS
 327 dNBR from GFBS, at around 100 (associated with representing represent as the low severity) and 700 (associated
 328 with represent as high severity), for the annual maximum forest fire in 2006. MOSEV dNBR from MOSEV on the
 329 other hand shows a single peak distribution at around 500, indicating that MOSEV dNBR from MOSEV
 330 underestimated the high severity occurrences, and while overestimated the low severity ones, depicted compared
 331 in the with GFBS dNBR from GFBS dataset. For the annual maximum forest fire in 2013, although though the density
 332 plot presents two different peaks in the distributions offer both dNBR from GFBS and MOSEV, indicating a
 333 significant shift difference in the burn severity depicted in the two datasets dNBR, the corresponding corresponded
 334 dNBR values where at the peaks are located in the distribution differ. For GFBS dNBR from GFBS, the two peaks
 335 are around 0 and 900, representing the low and high severity, respectively, while for MOSEV dNBR from MOSEV
 336 they are around 400 and 600.



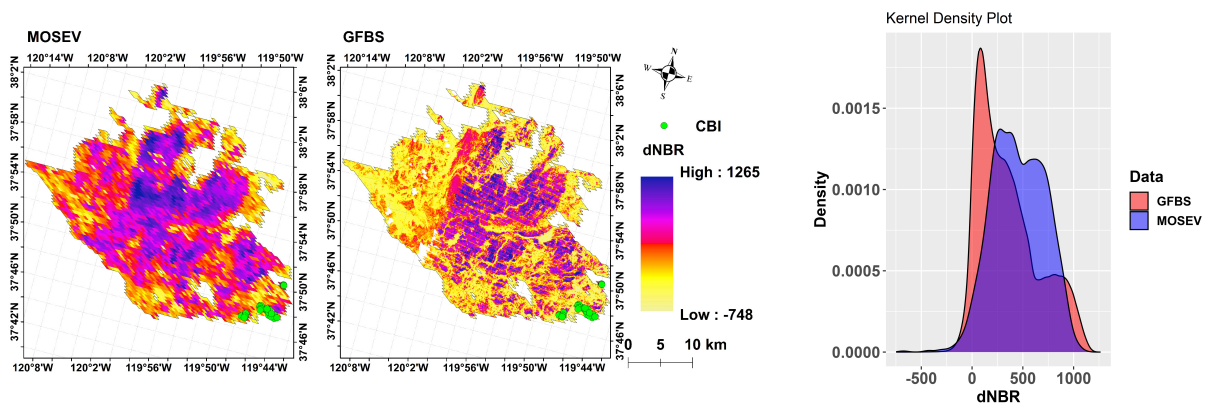
(a)



(b)



(c)

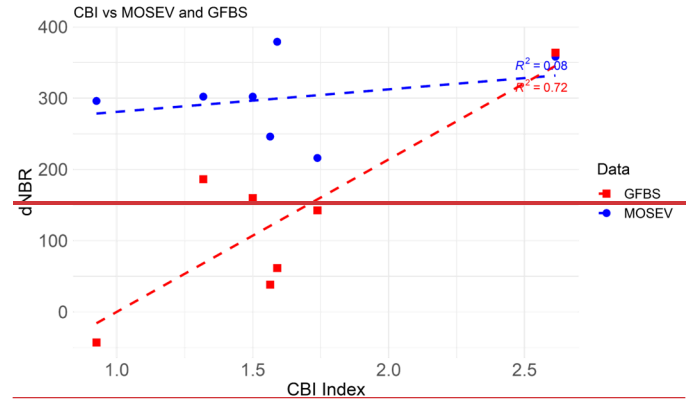
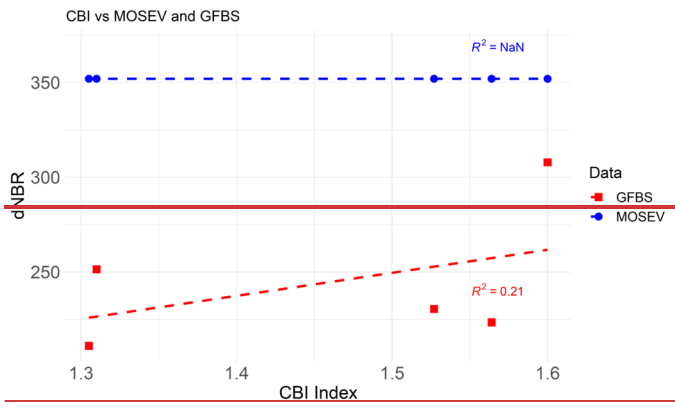
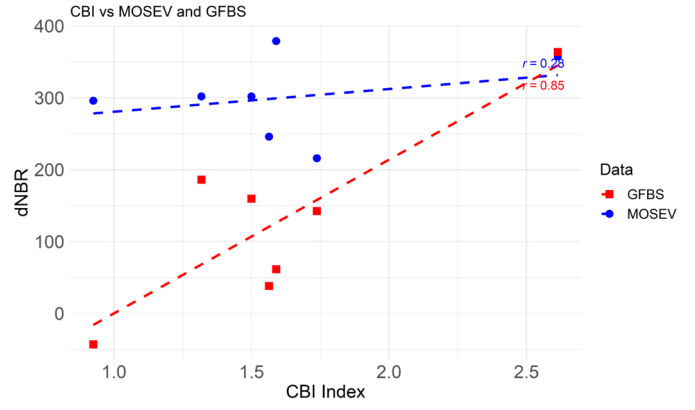
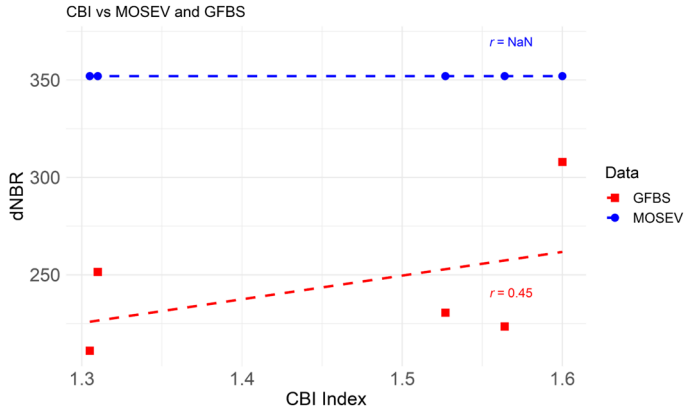


(d)

Figure 412. Spatial patterns of dNBRs for annual maximum fires over CONUS with distribution of probability density functions in (a) 2004, (b) 2006, (c) 2007, and (d) 2013, derived from the GFBS and MOSEV datasets.

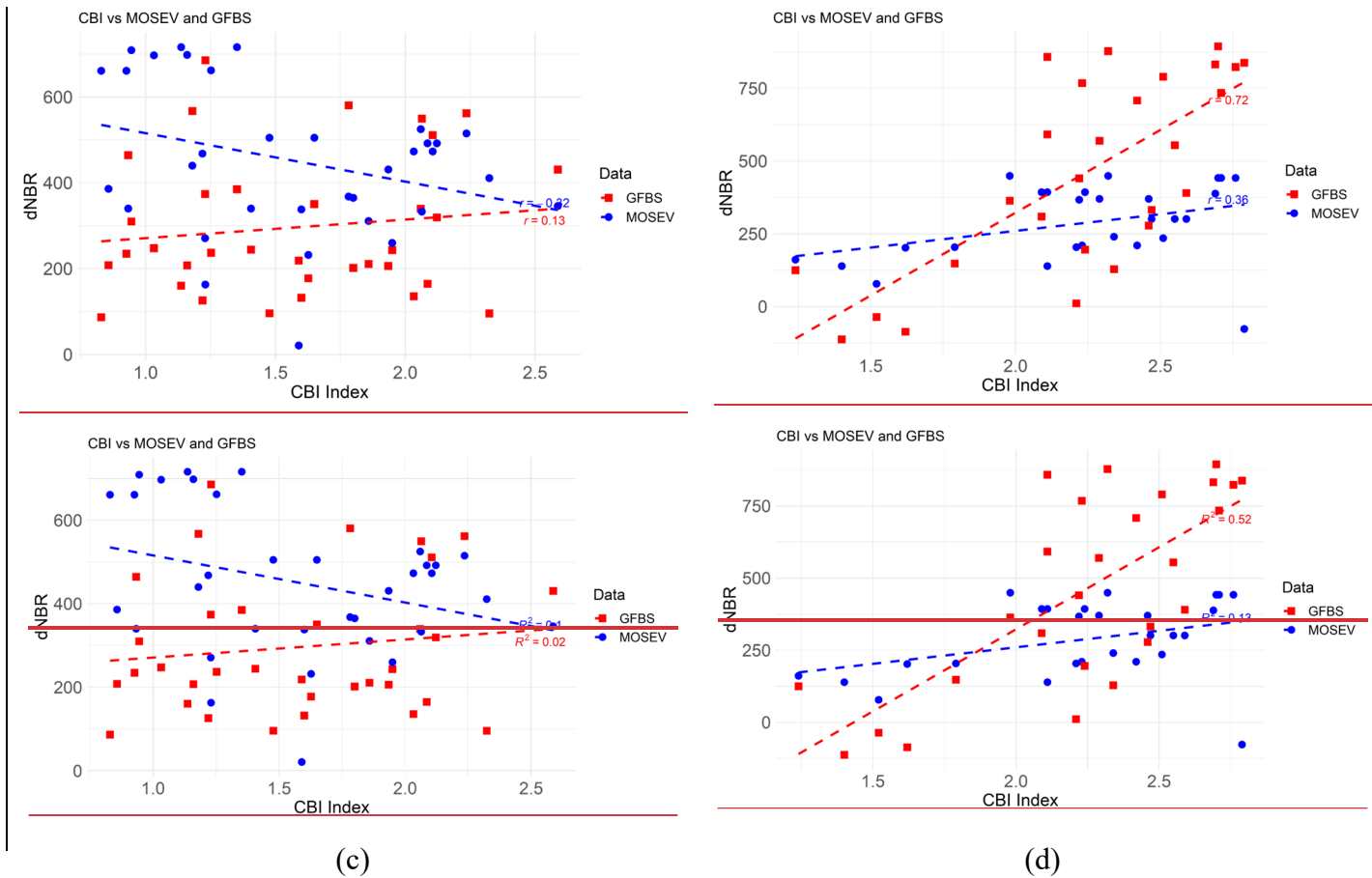
337
338
339
340
341
342
343
344
345
346
347
348

Figure 513, panels (a), (b), (c), and (d), present the scatterplots of CBI against GFBS-dNBR from GFBS and MOSEV-dNBR from MOSEV for the annual maximum forest fires in 2004, 2006, 2007, and 2013, respectively. For the annual maximum forest fire in 2004, the figure Figure 13 (a) clearly shows a positive correlation with-between CBI ($R^2-r = 0.2145$) for-and GFBS-dNBR from GFBS, while we found no correlation for-between CBI and MOSEV dNBR from MOSEV. For the annual maximum forest fire in 2006, we found good agreement with-between the CBI for-and GFBS-dNBR from GFBS, with an-a R^2-r value of 0.7285, while the R^2-r value was only 0.0828 for MOSEV dNBR from MOSEV. Although-Though correlations with-between CBI was poor for-bothand dNBR from GFBS and MOSEV were poor, -dNBR from GFBS for-the annual maximum forest fire in 2007, the former still showed a positive trend to CBI, while the relationship for-between CBI and dNBR from MOSEV the-latter was negative, for-the annual maximum forest fire in 2007. For the annual maximum forest fire in 2013, GFBS-dNBR from GFBS ($R^2-r = 0.5272$) was more strongly correlated with CBI than MOSEV-dNBR from MOSEV ($R^2-r = 0.1336$).



(a)

(b)



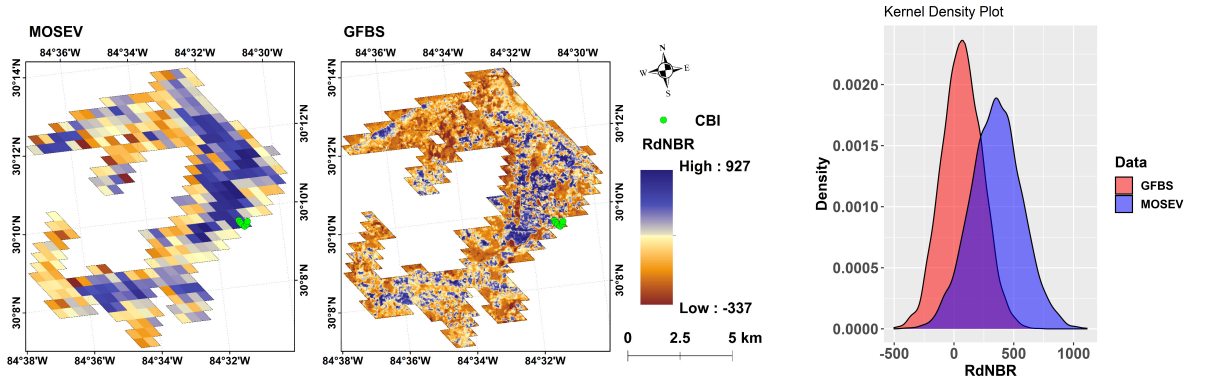
349 **Figure 513.** Scatterplots of CBI against dNBR ~~of~~ from GFBS and MOSEV for annual maximum fires in (a)
 350 2004, (b) 2006, (c) 2007, and (d) 2013.

351

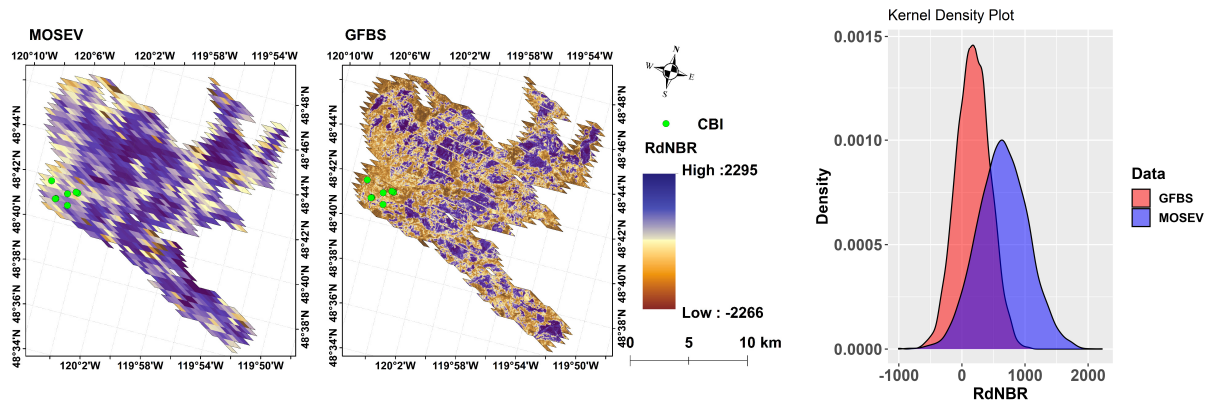
352

353 Figure 6-14 (a), (b), (c) and (d) shows the spatial patterns of RdNBR from GFBS and MOSEV along with
 354 the associated PDFs of RdNBR, for the forest fires over CONUS with the largest burn areas (referred to as annual
 355 maximum forest fire hereafter) in 2004, 2006, 2007, and 2013 respectively. ~~for which recorded CBIs are available.~~
 356 Like Figure 4, Figure 6 displays the spatial distribution maps of RdNBR from GFBS and MOSEV, along with the
 357 associated probability density functions (PDFs) of RdNBR values. The figure RdNBR from GFBS and MOSEV
 358 exhibits similar spatial patterns for GFBS and MOSEV dataset, but yet provide the burn severity level in terms of
 359 RdNBR differed different ranges range of RdNBR values over burn area. RdNBR ~~for~~ from MOSEV data tended to be
 360 higher than RdNBR from GFBS dNBR, which is consistent to the can could be clearly seen found in the density
 361 plots of RdNBR from GFBS, and MOSEV. The mean value in the distribution of RdNBRs from MOSEV that the
 362 mean RdNBR in the distribution of MOSEV is is larger is obviously larger than the mean value in the distribution of
 363 RdNBRs from GFBS the mean RdNBR in the distribution of GFBS, for the annual maximum forest fires in 2003, 2006
 364 and 2007. The density plots of RdNBR from GFBS and MOSEV RdNBR for the annual maximum forest fire in 2013

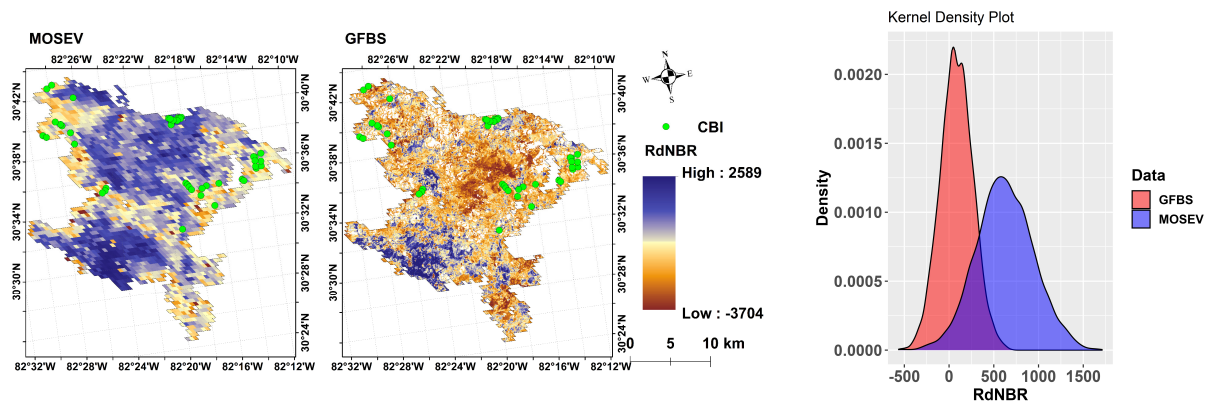
365 are largely overlapped for the annual maximum forest fire in 2013, but MOSEV-RdNBR from MOSEV distributes
 366 distributed more on the mean values around 800 than GFBS-RdNBR from GFBS, while GFBS-RdNBR from GFBS
 367 distributes-distributed more on the extreme low values above 0 and high values above 1500. These findings
 368 demonstrate that MOSEV-RdNBR from MOSEV represents overall higher-larger burn severity levels-estimations than
 369 GFBS-RdNBR from GFBS.



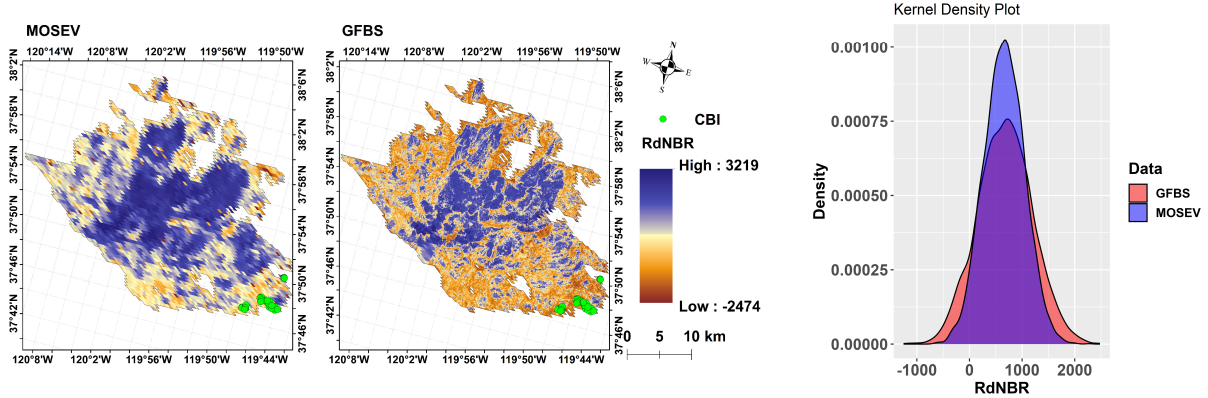
(a)



(b)



(c)



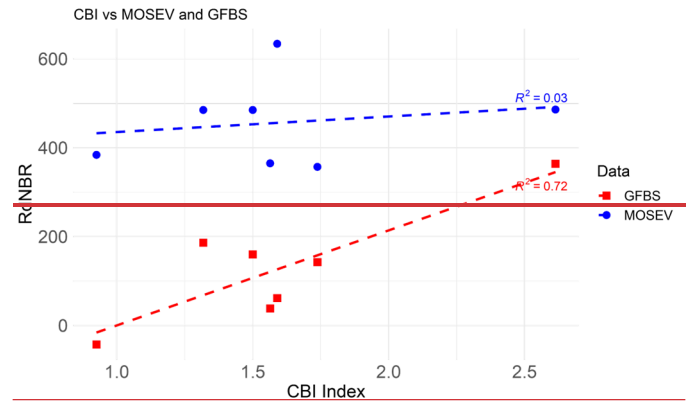
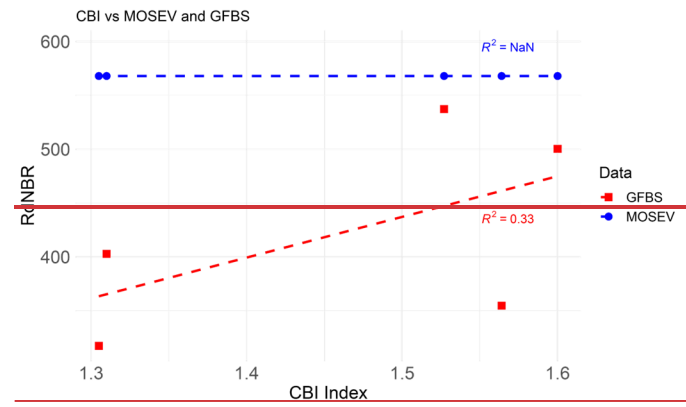
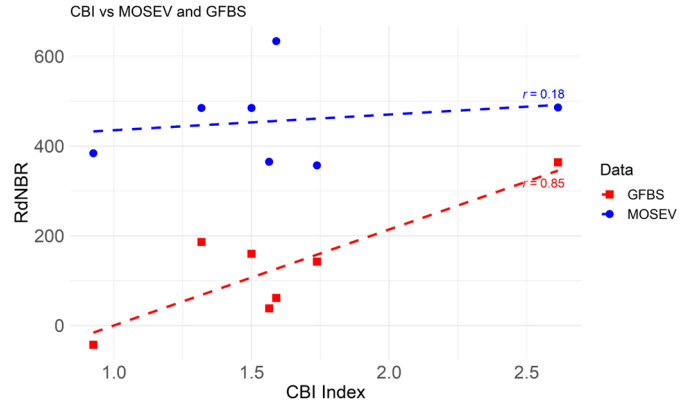
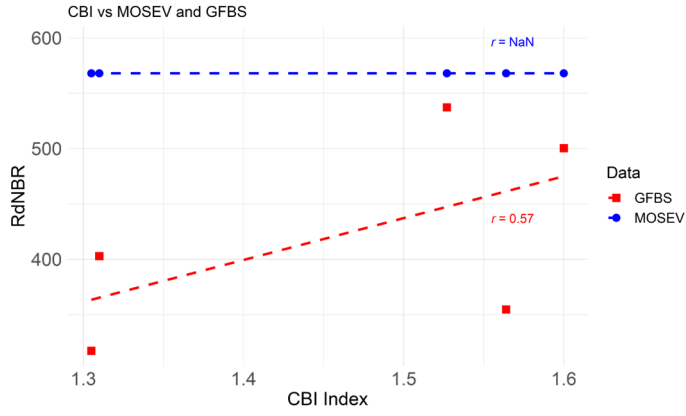
(d)

Figure 614. Spatial patterns of RdNBRs for annual maximum fires over CONUS with distribution of probability density functions in (a) 2004, (b) 2006, (c) 2007, and (d) 2013, derived from the GFBS and MOSEV datasets.

370

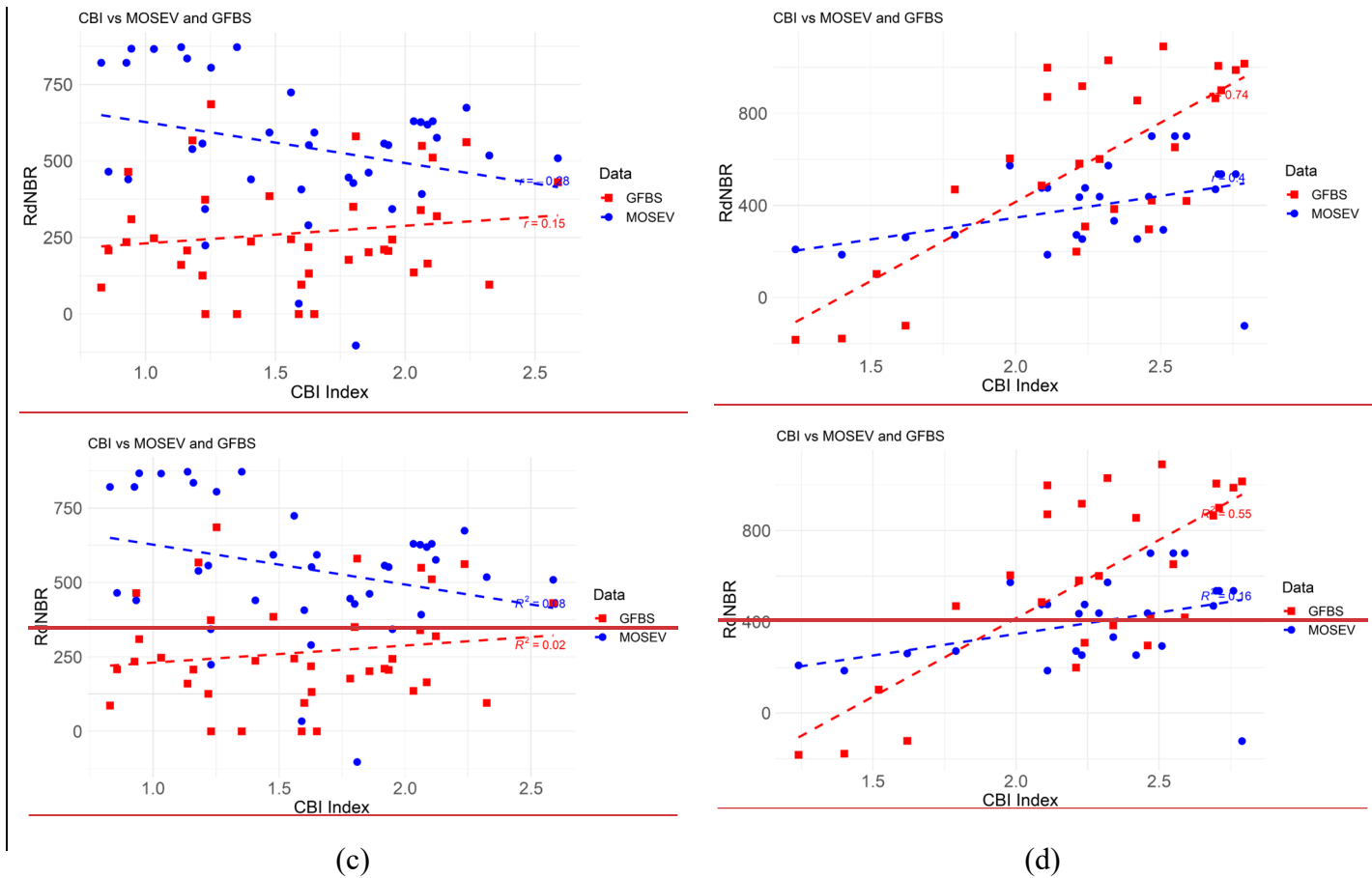
371 Figure 715, panels (a), (b), (c), and (d), present the scatterplots of CBI against ~~GFBS-RdNBR~~ RdNBR from GFBS
 372 and MOSEV, ~~RdNBR~~ RdNBR from MOSEV for the annual maximum forest fires in 2004, 2006, 2007, and 2013, respectively. For the annual
 373 maximum forest fire in 2004, ~~the figure~~ RdNBR from GFBS shows a positive correlation with CBI ($R^2-r = 0.3357$) ~~for~~
 374 ~~GFBS-dNBR~~, while ~~we found~~ no correlation was found between CBI and ~~for~~ RdNBR from MOSEV ~~dNBR~~. For the
 375 annual maximum forest fire in 2006, ~~we found good~~ RdNBR from GFBS correlated well ~~agreement~~ with the CBI for
 376 ~~GFBS-dNBR~~ with showing an a R^2-r value of 0.7285, while the R^2-r value was only 0.03-18 ~~for~~ between CBI and
 377 RdNBR from MOSEV ~~dNBR~~. ~~Although~~ The correlations with between CBI ~~was poor for both~~ and RdNBR from GFBS
 378 and MOSEV ~~dNBR~~ are bad for the annual maximum forest fire in 2007, the RdNBR from GFBS ~~former still~~ showed
 379 a positive trend to CBI with $r = 0.15$, while the RdNBR from MOSEV ~~showed a negative trend to CBI with~~ $r = -$
 380 0.28 ~~relationship for the latter was negative~~. For the annual maximum forest fire in 2013, GFBS-RdNBR from GFBS
 381 ($R^2-r = 0.5574$) was more strongly correlated with CBI than RdNBR from MOSEV ~~dNBR~~ ($R^2-r = 0.1640$).

382



(a)

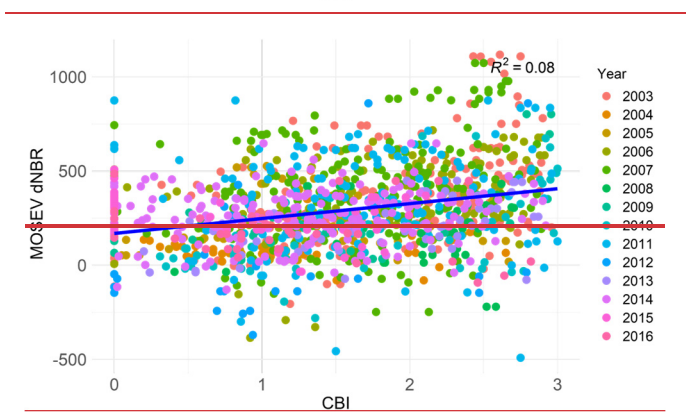
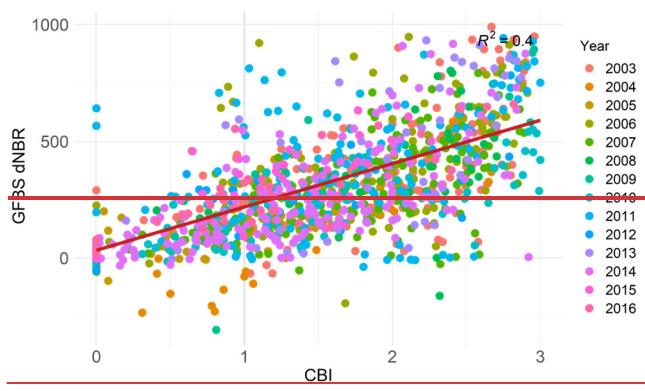
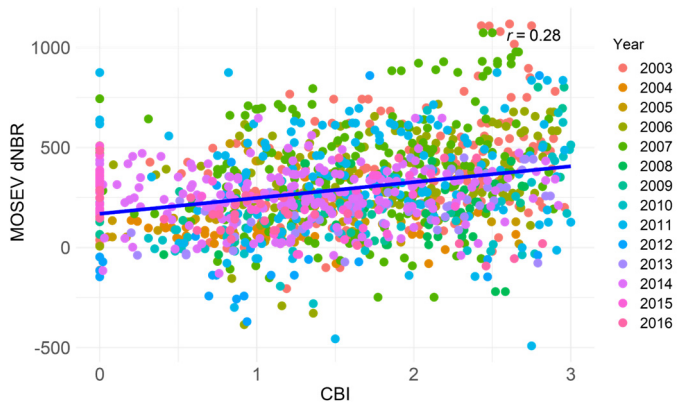
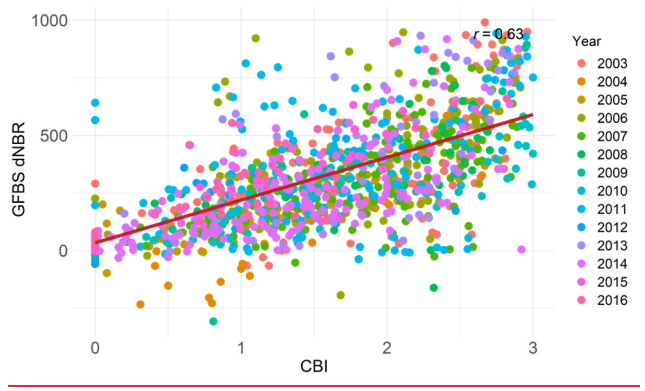
(b)



383 **Figure 715.** Scatterplots of CBI against RdNBR ~~of~~ from GFBS and MOSEV for annual maximum fires in (a)
 384 2004, (b) 2006, (c) 2007, and (d) 2013.

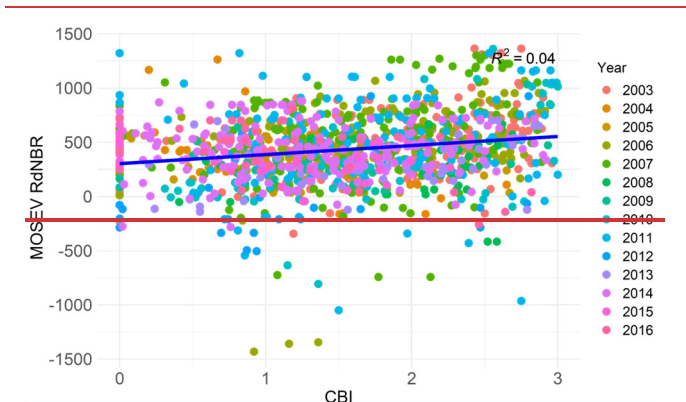
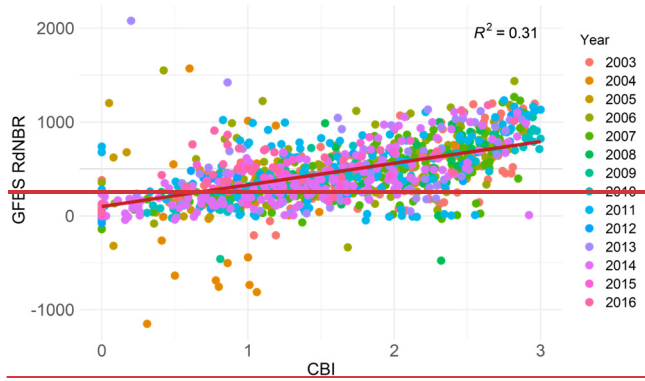
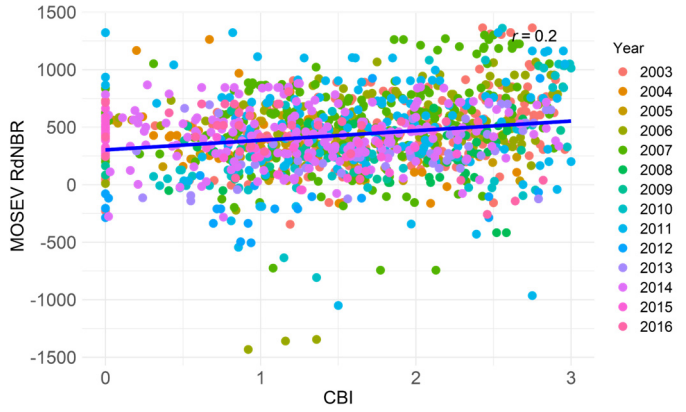
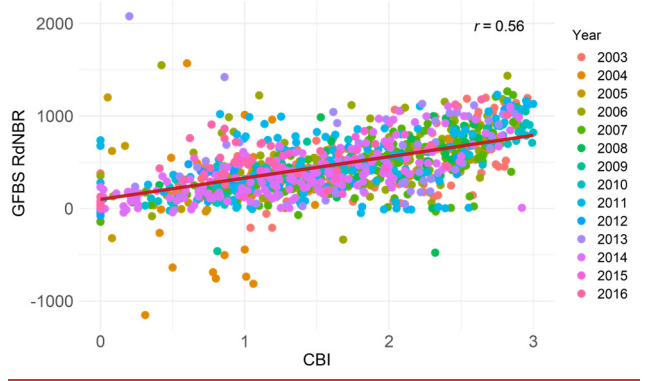
385

386 Figure 8-16 (a) and (b) shows the scatterplots of CBI against GFBS dNBR from GFBS and MOSEV dNBR,
 387 respectively, for all forest fires from 2003 to 2016 over CONUS. Considering all forest fires involving all ground
 388 validations, we found GFBS dNBR shows more strongly a stronger correlated correlation with CBI ($R^2-r = 0.463$) than
 389 MOSEV MOSEV dNBR ($R^2-r = 0.0828$). Using RdNBR as the burn severity, Figure 8-16 (c) and (d) show that GFBS
 390 RdNBR ($r=0.56$) still outperformed MOSEV RdNBR ($r=0.20$).



(a)

(b)



(c)

(d)

Figure 816. Scatterplots of CBI against (a) dNBR ~~of from~~ GFBS, (b) dNBR ~~of from~~ MOSEV, (c) RdNBR ~~of from~~ GFBS, and (d) RdNBR ~~of from~~ MOSEV for ~~all~~ forest fires from 2003 to 2016 over CONUS.

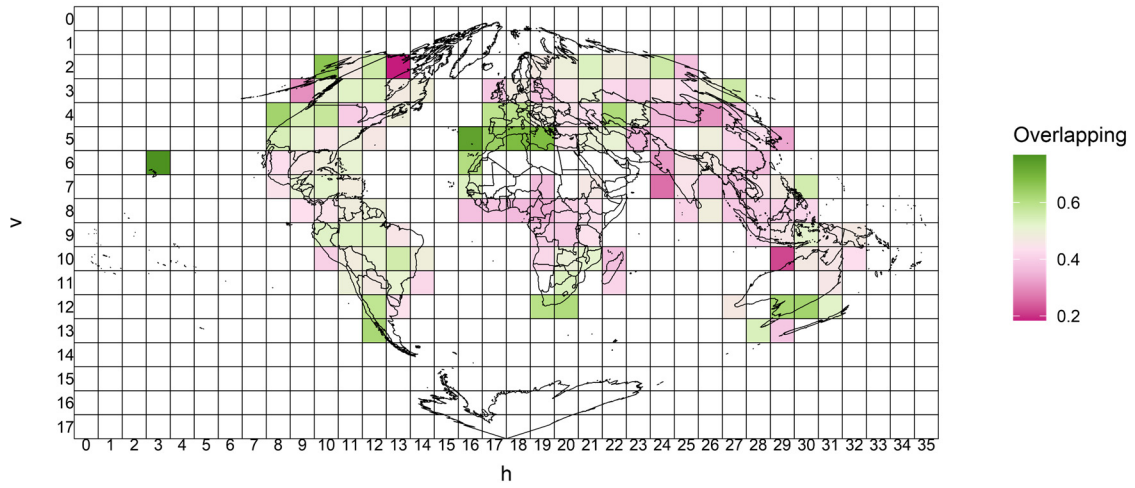
392

393 3.35. Comparison of GFBS and MOSEV globally

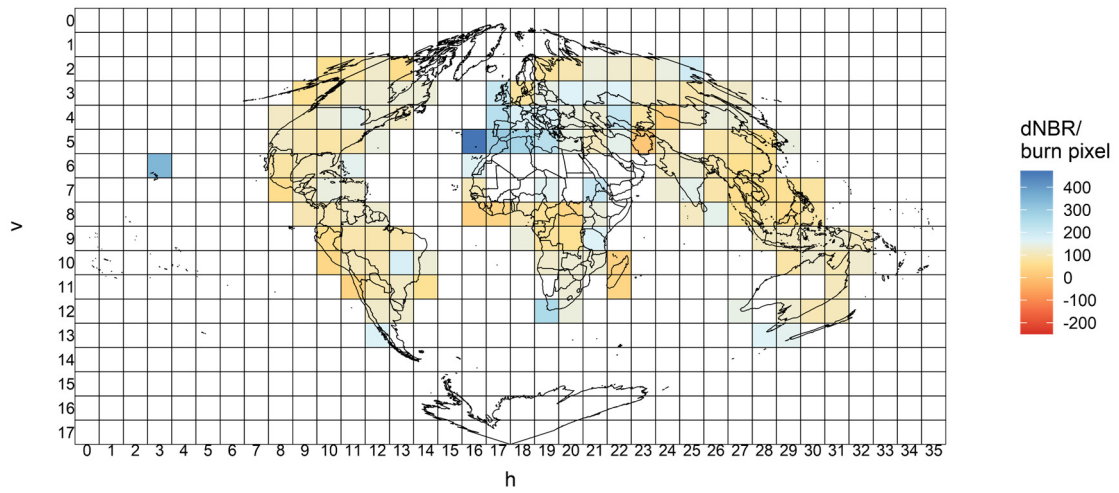
394 Figure 9-17 (a) displays the global spatial distributions of the ~~areas of overlap~~ overlapping area between the density
395 plots of ~~dNBR from~~ GFBS ~~dNBR~~ and MOSEV ~~dNBR~~, which is defined as the area intersected by two probability
396 density functions presented in Figure 4-12 and Figure 614. The overlapping areas in density plots typically represent
397 the percentage of common values between the distributions of two datasets, which ranges from 0 to 1 with the larger
398 value indicating the two distributions are more likely come from the same distribution. As ~~the figure~~ Figure 17 (a)
399 shows, we found the overlapping area over most of the world to be above 0.4, indicating a ~~close~~ similarity of 40%
400 between the burn severity information provided, ~~respective ly~~, by GFBS and MOSEV in these regions. For some
401 regions, like South America, Western Europe, and southeast Australia, the overlap was above 0.6.

402 ~~From~~ Figure 9-17 (b), which shows the global distribution of the mean dNBR for each burn pixel derived
403 from GFBS, ~~it is obvious that~~ we found the global spatial heterogeneity of burn severity to be small, with dNBR values
404 ~~from GFBS~~ around 100 and 200. The exception was ~~in~~ Western Europe, where dNBR was above 300. The global
405 distribution of the mean dNBR for each burn pixel derived from MOSEV, as shown in Figure 9-17 (c), however,
406 indicated a large spatial variability in burn severity ~~globally~~. The MOSEV dataset, for example, indicated that the
407 forest fires in north CONUS and Canada should have ~~the an~~ average dNBR ~~value~~ above 300, while in the GFBS
408 dataset the average dNBR value was around 100 to 200. The MOSEV dataset also indicated the average dNBR values
409 for forest fires in South Africa and China should be close to or below 0, while in the GFBS dataset they were around
410 100 to 200, ~~respectively~~.

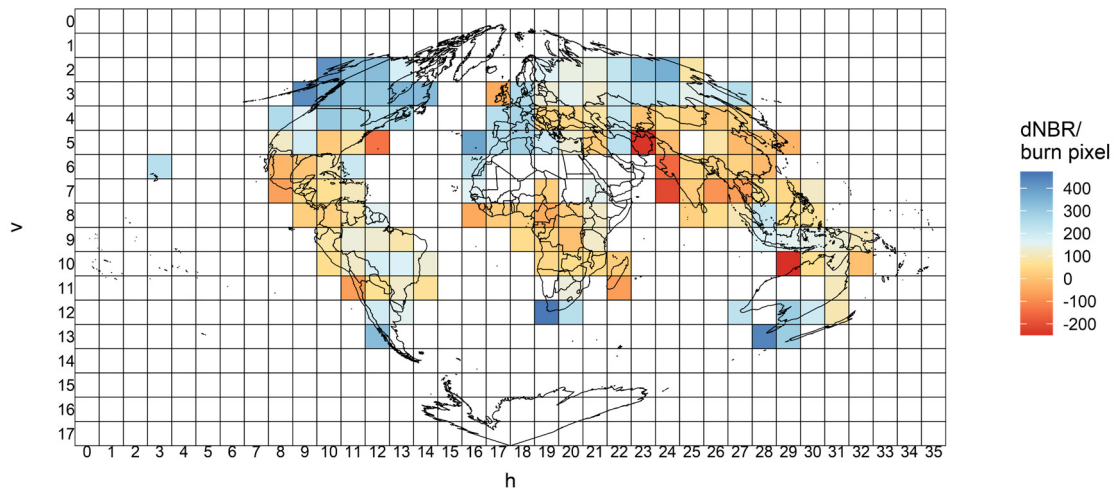
411 Figure 9-17 (d) presents a more detailed comparison between the ~~dNBR from~~ GFBS ~~dNBR~~ and MOSEV
412 ~~dNBR~~ globally, showing the difference in the mean dNBR for each burn pixel, as calculated by ~~MOSEV dNBR from~~
413 ~~MOSEV~~ minus ~~dNBR from~~ GFBS ~~dNBR~~. Globally, MOSEV data indicated higher forest burn severity ~~than GFBS~~
414 over ~~Canada and~~ CONUS ~~and Canada~~, also found in the results presented in section 3.2 and 3.4, as well as southeast
415 Australia ~~(also found in the results presented in section 3.3) than shown by GFBS data~~. MOSEV data presented lower
416 forest burn severity over Mexico, South Africa, Europe, China, and Southeast Asia. These findings revealed that the
417 forest burn severity information provided by GFBS might be ~~less under or overestimated~~ more reliable and reasonable
418 than that provided by MOSEV for some fire-prone areas, such as CONUS, as validated in this study. ~~The finding~~
419 ~~could also be applicable to other regions, including Canada, South Africa, and Australia~~. This improved accuracy over
420 MOSEV data would support advances in decision making in fire management strategies and ecosystem conservation
421 efforts.



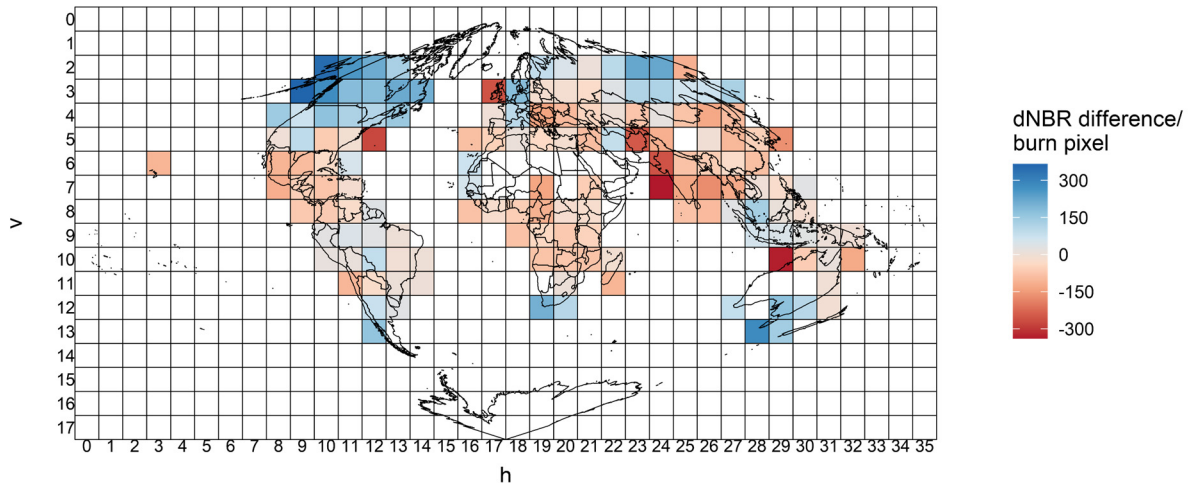
(a)



(b)



(c)



(d)

Figure 917. Global spatial distributions of (a) overlapping areas between the density plots of **GFBS-dNBR from GFBS** and **MOSEV-dNBR**, (b) the mean dNBR per burn pixel from GFBS, (c) the mean dNBR per burn pixel from MOSEV, and (d) the differences in the mean dNBR per burn pixel between MOSEV and GFBS (MOSEV – GFBS).

422

423 **4. Discussion**

424 ~~Our~~The GFBS dataset presented in this paper is the first to provide fine spatial resolution (30m) burn severity
 425 information for global forest fires from 2003 to 2016. Compared with the existing Landsat based CanLaBS dataset,
 426 GFBS shows closer agreement to CanLaBS in describing the distribution of annual forest fire burn severity than the
 427 MODIS based MOSEV data. As suggested by the validation against the ~~CBI~~ ground reference, GFBS can ~~capture~~
 428 better represent the more spatial variability and provide higher performance than the MOSEV dataset. In addition,
 429 GFBS is shown to have ~~less over- or underestimation~~ more reliable burn severity estimations than MOSEV for some
 430 fire-prone areas, like CONUS, Canada, ~~South Africa~~, and Australia, which could support advances in decision making
 431 in fire management strategies and ecosystem conservation efforts.

432 The difference in the performance of GFBS and MOSEV with respect to burn severity can be attributed to
 433 two sources. The first is ~~the spatial~~ spatial resolution. GFBS, based on Landsat (5, 7, and 8) images, is at a resolution
 434 of 30 meters, while MOSEV is based on MODIS Terra MOD09A1 and Aqua MYD09A1 images with a resolution of
 435 500 meters. As shown in Figure 11 (a), stemming from the coarse spatial resolution, MOSEV provides dNBR value
 436 of 295 for the site classified as high severity as well as for those classified as low severity, leading to an overestimation
 437 for low severity sites. ~~With~~ While with the improved spatial resolution, GFBS is able to capture more detailed localized
 438 variability of dNBR, providing more reasonable dNBR estimation for low severity sites (dNBR equal to 9, 16, 68).
 439 Similarly, in the event shown in Figure 11 (b), MOSEV provides dNBR estimations of 287 and 327 for the low severity
 440 sites, which is relatively too large. In GFBS, the relative lower dNBR of 30 and 32 is provided at the corresponding
 441 low severity ~~We based GFBS on Landsat (5, 7, and 8) images with a resolution of 30 meters, while MOSEV is based~~

442 ~~on MODIS Terra MOD09A1 and Aqua MYD09A1 images with a resolution of 500 meters. GFBS dNBR varies from~~
443 ~~210 to 310, showing a better correlation with CBI than MOSEV. The sites. The~~ coarse resolution of MOSEV could
444 also make it more difficult to capture ~~the~~ extreme values, as we found to be the case for the annual maximum forest
445 fires in 2006 over CONUS. ~~GFBS dNBR from GFBS~~ clearly showed two peaks in the density plot of dNBR at around
446 100 and 700, representing the low and high severity, respectively. ~~MOSEV dNBR from MOSEV~~, however, showed
447 only a single peak at around 500, indicating that the extreme low/high values in the 30m grid were averaged in the
448 500m grid. These findings reveal that burn severity from MOSEV has higher uncertainty for wildfires with larger
449 spatial variabilities.

450 Another reason leading to ~~the~~ the difference in the performances of the two data sets was related to sensors
451 onboard Landsat and MODIS. MODIS has a wider spectral range and more spectral bands (36) than Landsat 7/8 (7
452 spectral bands/ 11 spectral bands, respectively), which resulted in different sensitivity to surface reflectance. For
453 example, ~~spectrum reflectance information.~~ tThe NBR is commonly calculated using near-infrared (NIR) and
454 shortwave infrared (SWIR) bands. In MOSEV, the bands used to calculate NBR are NIR: Band 2 (Range: 0.841–
455 0.876 μm) and SWIR: Band 7 (Range: 2.105–2.155 μm). In GFBS, they are Landsat 5 Band 4 (Range: 0.76–0.90 μm)
456 and SWIR: Band 7 (Range: 2.08–2.35 μm); Landsat 7 Band 4 (Range: 0.77–0.90 μm) and SWIR: Band 7 (Range:
457 2.09–2.35 μm); and Landsat 8 Band 5 (Range: 0.85–0.88 μm) and SWIR: Band 7 (Range: 2.11–2.29 μm). While
458 MODIS and Landsat 8 are close in NIR and SWIR band information, Landsat 5 and 7 both have wider spectrums in
459 NIR and SWIR than MODIS.

460 This study has shown that ~~using and~~ combining all available Landsat images, including those from Landsat
461 5, 7, and 8, could significantly improve the probability of obtaining dense cloud-free NBR time series. The NBR
462 composite shows high spatial and temporal consistency with the NBR images closest to the start and end time of the
463 fire event, despite different band settings used from Landsat 5, 7 and 8. Studies by Koutsias and Pleniou (2015) and
464 Chen et al. (2020) also ~~have shown~~ that differences are small when using reflectance values from sensors aboard the
465 Landsat 5, 7, and 8 satellites to calculate burn severity over burned area. While studies (Mallinis et al., 2018; Howe et
466 al. 2022) have demonstrated that Sentinel-2 generally performed as well as Landsat 8 in burn severity mapping, the
467 further extension of this study will also incorporate images from Sentinel-2 to obtain dNBR composite, especially on
468 extending the GFBS data set to the present. With the finer spatial resolution (10 meter) and more frequent revisit
469 period (5 days), GFBS could provide improved burn severity information when incorporating Sentinel-2 images. The
470 National Aeronautics and Space Administration (NASA) has ~~launched~~ ~~initiated~~ the Harmonized Landsat and Sentinel-
471 2 (HLS) project aiming to produce a seamless surface reflectance record from the Operational Land Imager (OLI) and
472 Multi-Spectral Instrument (MSI) aboard Landsat-8/9 and Sentinel-2A/B remote sensing satellites, respectively, which
473 is an alternative source for extending the GFBS dataset (<https://hls.gsfc.nasa.gov/>)

474 With the development of radar-based techniques, Synthetic Aperture Radar (SAR) polarimetric images have
475 been proven to be effective in burn severity mapping, owing to the strong correlation between SAR backscatter and
476 burn severity [Czuchlewski and Weissel, 2005; Tanase et al., 2010; Tanase et al., 2011; Addison and Oommen, 2018].
477 With the unique properties of L-band SAR, it is suitable for assessing and monitoring post-fire effects and burn

478 severity [Tanase et al., 2010; Peacock et al., 2023]. For example, the frequency of L-band (1.26 GHz) allows it to
479 penetrate through smoke, ash, and, to some extent, vegetation canopy. This capability makes L-band SAR particularly
480 useful for assessing areas immediately after a fire, even in the presence of smoke or cloud cover that would obstruct
481 optical sensors. The incorporation of L-band Synthetic Aperture Radar (SAR) data, such as the ALOS-2 PALSAR-2
482 ScanSAR Level 2.2 data (https://www.eorc.jaxa.jp/ALOS/en/alos-2/a2_about_e.htm) and the incoming NASA-
483 ISRO Synthetic Aperture Radar (NISAR, <https://nisar.jpl.nasa.gov/>), can also facilitate the retrieval of burn severity.

484 By comparing GFBS with CanLaBS, we found that the number of forest fires in CanLaBS dataset is larger
485 than those in GFBS. This is because CanLaBS is based on the burn area map from Canada Landsat Disturbance
486 product at 30 meter resolution, while GFBS is based on the burn area map from Global Fire Atlas which is derived
487 from MODIS burn area product at 500 meter resolution. This difference in the spatial resolution of the burn area
488 area causes some small forest fires to be ignored in the GFBS dataset. Therefore, finer spatial
489 resolution burn area product (10/30 meter) is promoted regionally and globally to better reveal the forest fire behavior,
490 e.g. fire number, size and severity (Roy et al., 2019; Bar et al., 2020). Despite the differences in number of forest fires,
491 GFBS agreed well to CanLaBS in terms of the annual forest burn severity. While the method to generate GFBS
492 remains consistent, with the small difference to be ignored in banding settings from Landsat 5, 7 and 8, GFBS provides
493 comprehensive temporal coverage spanning from 2003 to 2016 for forest burn severity, indicating the potential
494 application of GFBS in long term analysis of burn severity for forest fires beyond Canada, i.e. regions over the globe,
495 e.g. CONUS, Australia, where GFBS has been demonstrated to perform well against ground truth. Moreover,
496 integrating the 30 meter GFBS into the regional forest planning can enhance fire resilience in vulnerable areas, shaping
497 policies that prioritize the forest environment [Bradley et al., 2016]. As climate change exacerbates the frequency,
498 intensity, and unpredictability of wildfires globally, the analysis on GFBS data can help to assess the impact of these
499 fires on carbon emissions [Xu et al., 2020], forest recovery [Meng et al., 2018], and biodiversity [Huerta et al., 2022],
500 which would in turn inform predictive models that project future fire behavior under various climate scenarios.

501
502 One limitation of the GFBS database is related to the relatively long revisit period of Landsat satellites (16
503 days). This low temporal resolution may impede us from obtaining the dense cloud-free NBR time series that can be
504 indispensable to calculating burn severity indices in regions of persistent cloud cover. This study has shown, however,
505 that using and combining all available Landsat images, including those from Landsat 5, 7, and 8, could significantly
506 improve the probability of obtaining dense cloud-free NBR time series. With the launch of Landsat 9 in September
507 2021 and other satellites like Sentinel 2 (in June 2015, with a five-day revisit period), it is highly possible that we
508 could build a denser cloud-free NBR time series to calculate burn severity.

509 A second limitation of GFBS is that it uses different band information varies in spectrum range from Landsat
510 5, 7, and 8, which might cause data quality to differ across years, while MOSEV uses the same bands in all years,
511 showing better data consistency.

512 5. Conclusion

513 We have introduced a newly developed [dataset-GFBS database, named GFBS](#), which provides forest burn severity
514 information with global coverage for the period 2003–2016. We identified global forest fires by overlaying the Global
515 Fire Atlas data with the annual land cover data, MCD12Q1, and proposed an automated algorithm for calculating the
516 severity of these fires. The algorithm used the band information from Landsat 5, 7, and 8 surface reflectance imagery
517 to compute the most used burn severity spectral indices (dNBR and RdNBR) with a 30m spatial resolution and provide
518 the output ~~depicted in theas the~~ GFBS dataset. [Comparison between CanLaBS and GFBS showed good](#)
519 [agreementindicateds that GFBS agreed well in representing the distribution of forest burn severity to those of](#)
520 [CanLaBS over Canada. The validation against field assessed burn severity category data in southeastern Australia](#)
521 [showed that GFBS could provide burn severity estimation with clear differentiation discrepancy between the high-](#)
522 [severity class and moderate/low severity class of the in situ data, while such differences among burn severity class](#)
523 [were are-not obvious in the MOSEV dataset.](#) The validation results over CONUS showed dNBR ~~of values from~~ GFBS
524 ~~to be~~ more strongly correlated with CBI ($R^2-r = 0.463$) than dNBR ~~fromof~~ MOSEV ($R^2-r = 0.0828$). RdNBR ~~of from~~
525 ~~GFSS-GFBS~~ also showed better agreement with CBI ($R^2-r = 0.3456$) than RdNBR ~~of from~~ MOSEV ($R^2-r = 0.0420$).
526 Thus, this database could be more reliable than prior sources of information for future studies of forest burn severity
527 at ~~the~~ global scale ~~in a computationally cost effective way~~, as well as for studies to which forest burn severity could
528 be relevant, such as in forest management and ~~CO²-CO₂~~ emissions research.

529 ~~A One~~ future direction for this study ~~would will~~ be to extend the GFBS dataset to the present based on
530 updated Global Fire Atlas data or other datasets providing [global similar](#) burn area and burn date information. ~~A another~~
531 [direction second](#) is to [involve more ground validations from the fire prone areas like south Africa and south Mexico](#)
532 [to further evaluate and improve the performances of GFBS data globally.](#)

533 ~~show the similar spatial patterns in presenting burn severity from GFBS and MOSEV dataset, the less~~
534 ~~over/underestimated GFBS data could serve as an optional input for adjusting the bias in MOSEV data and take the~~
535 ~~advantage of high spatial resolution of GFBS data, the spatial downscaling of MOSEV data is applicable in regions~~
536 ~~where GFBS and MOSEV show high consistency.~~

537 **Competing interests:** The authors declare they have no conflict of interest.

538 **Data availability:** The GFBS data are freely accessible at <https://doi.org/10.5281/zenodo.10037629> (He et al., 2023)

539 **Author contributions:** KH and EA designed and organized the manuscript. KH and XS prepared the related materials
540 and ran the models for generating GFBS and the related assessments. XS and EA made contributions to the scientific
541 framework of this study and discussed the interpretation of the results. All authors discussed the results and
542 commented on the manuscript.

543 **Acknowledgments:** This research was supported by a National Science Foundation HDR award entitled
544 “Collaborative Research: Near Term Forecast of Global Plant Distribution Community Structure and Ecosystem
545 Function.” Kang He received the support of the China Scholarship Council for four years’ Ph.D. study at the University
546 of Connecticut (under grant agreement no. 201906320068). [Thanks for Rachael Gallagher and Eli Bendall from](#)
547 [Western Sydney University for sharing the field assessed fire severity category data over southeastern Australia.](#)

548 **Reference:**

549 Abreu, R.C., Hoffmann, W.A., Vasconcelos, H.L., Pilon, N.A., Rossatto, D.R. and Durigan, G.: The biodiversity cost
550 of carbon sequestration in tropical savanna, *Sci. Adv.*, 3, e1701284, <https://doi.org/10.1126/sciadv.1701284>, 2017.

551 [Alcaras, E., Costantino, D., Guastaferrero, F., Parente, C., Pepe, M.: Normalized Burn Ratio Plus \(NBR+\): A New Index
552 for Sentinel-2 Imagery. *Remote Sens.*, 14, 1727. <https://doi.org/10.3390/rs14071727>, 2022.](#)

553 Alonso-González, E. and Fernández-García, V.: MOSEV: a global burn severity database from MODIS (2000–2020),
554 *Earth Syst. Sci. Data*, 13, 1925–1938, <https://doi.org/10.5194/essd-13-1925-2021>, 2021.

555 Andela, N., Morton, D. C., Giglio, L., Paugam, R., Chen, Y., Hantson, S., van der Werf, G. R., and Randerson, J. T.:
556 The Global Fire Atlas of individual fire size, duration, speed and direction, *Earth Syst. Sci. Data*, 11, 529–552,
557 <https://doi.org/10.5194/essd-11-529-2019>, 2019.

558 Aragão, L.E., Anderson, L.O., Fonseca, M.G., Rosan, T.M., Vedovato, L.B., Wagner, F.H., Silva, C.V., Silva Junior,
559 C.H., Arai, E., Aguiar, A.P. and Barlow, J.: 21st Century drought-related fires counteract the decline of Amazon
560 deforestation carbon emissions, *Nat. Commun.*, 9(1), 536, <https://doi.org/10.1038/s41467-017-02771-y>, 2018.

561 Archibald, S. and Roy, D.P.: Identifying individual fires from satellite-derived burned area data, 2009 IEEE
562 International Geoscience and Remote Sensing Symposium, Cape Town, South Africa, 12-17 July 2009, 11150061,
563 <https://doi.org/10.1109/IGARSS.2009.5417974>, 2009.

564 [Bar, S., Parida, B.R. and Pandey, A.C. Landsat-8 and Sentinel-2 based Forest fire burn area mapping using machine
565 learning algorithms on GEE cloud platform over Uttarakhand, Western Himalaya. *Remote Sens Appl.*, 18, 100324,
566 <https://doi.org/10.1016/j.rsase.2020.100324>, 2020.](#)

567 Benali, A., Russo, A., Sá, A.C., Pinto, R.M., Price, O., Koutsias, N. and Pereira, J.M.: Determining fire dates and
568 locating ignition points with satellite data, *Remote. Sens.*, 8(4), 326, <https://doi.org/10.3390/rs8040326>, 2016.

569 [Chen D., Loboda T.V., and Hall J.V. A systematic evaluation of influence of image selection process on remote
570 sensing-based burn severity indices in North American boreal forest and tundra ecosystems. *ISPRS J. Photogramm.*
571 *Remote Sens.* 159, 63–77. <https://doi.org/10.1016/j.isprsjprs.2019.11.011>, 2020.](#)

572 Chuvieco, E., Aguado, I., Yebra, M., Nieto, H., Salas, J., Martín, M.P., Vilar, L., Martínez, J., Martín, S., Ibarra, P.
573 and De la Riva, J.: Development of a framework for fire risk assessment using remote sensing and geographic
574 information system technologies, *Ecol. Modell.*, 221(1), 46-58, <https://doi.org/10.1016/j.ecolmodel.2008.11.017>,
575 2010.

576 Chuvieco, E., Yue, C., Heil, A., Mouillot, F., Alonso-Canas, I., Padilla, M., Pereira, J.M., Oom, D. and Tansey, K.: A
577 new global burned area product for climate assessment of fire impacts, *Glob. Ecol. Biogeogr.*, 25(5), 619-629,
578 <https://doi.org/10.1111/geb.12440>, 2016.

579 [Cocke, A.E., Fulé, P.Z. and Crouse, J.E.: Comparison of burn severity assessments using Differenced Normalized](#)
580 [Burn Ratio and ground data. *Int J Wildland Fire*, 14\(2\), 189-198. <https://doi.org/10.1071/WF04010>, 2005.](#)

581 Doerr, S.H. and Santín, C.: Global trends in wildfire and its impacts: perceptions versus realities in a changing world,
582 *Phil. Trans. R. Soc. B.*, 371,1696, <http://doi.org/10.1098/rstb.2015.0345>, 2016.

583 Dupuy, J.L., Fargeon, H., Martin-StPaul, N., Pimont, F., Ruffault, J., Guijarro, M., Hernando, C., Madrigal, J. and
584 Fernandes, P.: Climate change impact on future wildfire danger and activity in southern Europe: a review, *Ann. For.*
585 *Sci.*, 77(2), 1-24, <https://doi.org/10.1007/s13595-020-00933-5>, 2020.

586 Eidenshink, J., Schwind, B., Brewer, K., Zhu, Z.L., Quayle, B. and Howard, S.: A project for monitoring trends in
587 burn severity, *Fire. Ecol.*, 3(1), 3-21, <https://doi.org/10.4996/fireecology.0301003>, 2007.

588 Flannigan, M.D., Amiro, B.D., Logan, K.A., Stocks, B.J. and Wotton, B.M.: Forest fires and climate change in the 21
589 st century, *Mitig. Adapt. Strat. Glob. Change.*, 11, 847-859, <https://doi.org/10.1007/s11027-005-9020-7>, 2006.

590 Flannigan, M.D., Stocks, B.J. and Wotton, B.M.: Climate change and forest fires, *Sci. Total. Environ.*, 262(3), 221-
591 229, [https://doi.org/10.1016/S0048-9697\(00\)00524-6](https://doi.org/10.1016/S0048-9697(00)00524-6), 2000.

592 Friedl, M. and Sulla-Menashe, D.: MODIS/Terra+Aqua Land Cover Type Yearly L3 Global 500m SIN Grid V061
593 [Data set], NASA EOSDIS Land Processes Distributed Active Archive Center,
594 <https://doi.org/10.5067/MODIS/MCD12Q1.061>, 2022.

595 Fusco, E.J., Abatzoglou, J.T., Balch, J.K., Finn, J.T. and Bradley, B.A.: Quantifying the human influence on fire
596 ignition across the western USA, *Ecol. Appl.*, 26(8),2390-2401, <https://doi.org/10.1002/eap.1395>, 2016

597 Guindon, L., Gauthier, S., Manka, F., Parisien, M.A., Whitman, E., Bernier, P., Beaudoin, A., Villemaire, P. and
598 Skakun, R.: Trends in wildfire burn severity across Canada, 1985 to 2015, *Can. J. For. Res.*, 51(9),1230-1244,
599 <https://doi.org/10.1139/cjfr-2020-0353>, 2021.

600 [Guindon, L., P. Villemaire, R. St-Amant, P.Y. Bernier, A. Beaudoin, F. Caron, M. Bonucelli and H. Dorion.: Canada](#)
601 [Landsat Disturbance \(CanLaD\): a Canada-wide Landsat-based 30-m resolution product of fire and harvest detection](#)
602 [and attribution since 1984. <https://doi.org/10.23687/add1346b-f632-4eb9-a83d-a662b38655ad>, 2017.](#)

603 [Guindon, L.; Bernier, P.Y.; Gauthier, S.; Stinson, G.; Villemaire, P.; Beaudoin, A.: Missing forest cover gains in](#)
604 [boreal forests explained. *Ecosphere*, 9 \(1\), e02094. <https://doi.org/10.1002/ecs2.2094>, 2018.](#)

605 Hantson, S., Pueyo, S. and Chuvieco, E.: Global fire size distribution is driven by human impact and climate, *Glob.*
606 *Ecol. Biogeogr.*, 24(1), 77-86, <https://doi.org/10.1111/geb.12246>, 2015.

607 He, K., Shen, X., & Anagnostou, E. N.: A Global Forest Burn Severity Dataset from Landsat Imagery (2003–2016)
608 [Data set], Zenodo, <https://doi.org/10.5281/zenodo.10037629>, 2023.

609 [Howe, A.A., Parks, S.A., Harvey, B.J., Saberi, S.J., Lutz, J.A. and Yocom, L.L. Comparing Sentinel-2 and Landsat 8](#)
610 [for burn severity mapping in Western North America. Remote Sensing, 14\(20\), 5249,](#)
611 <https://doi.org/10.3390/rs14205249>, 2022.

612 Jolly, W.M., Cochrane, M.A., Freeborn, P.H., Holden, Z.A., Brown, T.J., Williamson, G.J. and Bowman, D.M.:
613 Climate-induced variations in global wildfire danger from 1979 to 2013, Nat. Commun., 6, 7537,
614 <https://doi.org/10.1038/ncomms8537>, 2015.

615 Kasischke, E.S. and Turetsky, M.R.: Recent changes in the fire regime across the North American boreal region—
616 Spatial and temporal patterns of burning across Canada and Alaska, Geophys. Res. Lett., 33(9),
617 <https://doi.org/10.1029/2006GL025677>, 2006.

618 Keeley, J.E.: Fire intensity, burn severity and burn severity: a brief review and suggested usage, Int. J. Wildland. Fire.,
619 18(1), 116-126, <https://doi.org/10.1071/WF07049>, 2009.

620 [Key, C. H. and Benson, N.C.: The Normalized Burn Ratio \(NBR\): A Landsat TM radiometric measure of burn](#)
621 [severity, US Department of the Interior. US Geological Survey, Northern Rocky Mountain Science Center. 2003.](#)

622 Key, C.H. and Benson, N.C.: Landscape assessment (LA): Sampling and Analysis Methods, USDA Forest Service,
623 55 pp, 2006.

624 [Koutsias N. and Pleniou M. Comparing the spectral signal of burned surfaces between Landsat 7 ETM+ and Landsat](#)
625 [8 OLI sensors. Int. J. Remote Sens. 36\(14\), 3714–3732, https://doi.org/10.1080/01431161.2015.1070322, 2015.](#)

626 Laurent, P., Mouillot, F., Yue, C., Ciais, P., Moreno, M.V. and Nogueira, J.M.: FRY, a global database of fire patch
627 functional traits derived from space-borne burned area products, Sci. Data., 5(1), 1-12,
628 <https://doi.org/10.1038/sdata.2018.132>, 2018.

629 [Mallinis, G., Mitsopoulos, I. and Chrysafi, I. Evaluating and comparing Sentinel 2A and Landsat-8 Operational Land](#)
630 [Imager \(OLI\) spectral indices for estimating fire severity in a Mediterranean pine ecosystem of Greece. Gisci Remote](#)
631 [Sens, 55\(1\), 1-18, https://doi.org/10.1080/15481603.2017.1354803, 2018.](#)

632 Miller, J.D. and Thode, A.E.: Quantifying burn severity in a heterogeneous landscape with a relative version of the
633 delta Normalized Burn Ratio (dNBR), Remote. Sens. Environ., 109(1), 66-80,
634 <https://doi.org/10.1016/j.rse.2006.12.006>, 2007.

635 [Miller, J.D., Knapp, E.E., Key, C.H., Skinner, C.N., Isbell, C.J., Creasy, R.M. and Sherlock, J.W.: Calibration and](#)
636 [validation of the relative differenced Normalized Burn Ratio \(RdNBR\) to three measures of fire severity in the Sierra](#)
637 [Nevada and Klamath Mountains, California, USA. Remote Sens Environ, 113\(3\), 645-656,](#)
638 <https://doi.org/10.1016/j.rse.2008.11.009>, 2009.

639 [Montero, D., Aybar, C., Mahecha, M.D., Martinuzzi, F., Söchting, M. and Wieneke, S. A standardized catalogue of](#)
640 [spectral indices to advance the use of remote sensing in Earth system research. Sci Data 10, 197,](#)
641 <https://doi.org/10.1038/s41597-023-02096-0>, 2023.

642 Moreira, F., Ascoli, D., Safford, H., Adams, M.A., Moreno, J.M., Pereira, J.M., Catry, F.X., Armesto, J., Bond, W.,
643 González, M.E. and Curt, T.: Wildfire management in Mediterranean-type regions: paradigm change needed, Environ.
644 Res. Lett., 15, 011001, <https://doi.org/10.1088/1748-9326/ab541e>, 2020.

645 Nasi, R., Dennis, R., Meijaard, E., Applegate, G. and Moore, P.: Forest fire and biological diversity, UNASYLVA-
646 FAO., 36-40, 2002.

647 Nogueira, J.M., Ruffault, J., Chuvieco, E. and Mouillot, F.: Can we go beyond burned area in the assessment of global
648 remote sensing products with fire patch metrics?, Remote. Sens., 9(1), 7, <https://doi.org/10.3390/rs9010007>, 2016.

649 Oom, D., Silva, P.C., Bistinas, I. and Pereira, J.M.: Highlighting biome-specific sensitivity of fire size distributions to
650 time-gap parameter using a new algorithm for fire event individuation, Remote. Sens., 8(8), 663,
651 <https://doi.org/10.3390/rs8080663>, 2016.

652 Rodrigues, M. and Febrer, M.: Spatial-temporal modeling of forest fire behavior: modeling fire ignition and
653 propagation from MCD64A1, 20th EGU General Assembly, Vienna, Austria, 4-13 April, 2018,
654 2018EGUGA..2014568R, 2018.

655 [Roy, D.P., Huang, H., Boschetti, L., Giglio, L., Yan, L., Zhang, H.H. and Li, Z. Landsat-8 and Sentinel-2 burned area](#)
656 [mapping-A combined sensor multi-temporal change detection approach. Remote Sens Environ, 231, 111254,](#)
657 <https://doi.org/10.1016/j.rse.2019.111254>, 2019.

658 Scholes, R.J. and Archer, S.R.: Tree-grass interactions in savannas, Annu. Rev. Ecol. Syst., 28, 517-544,
659 <https://doi.org/10.1146/annurev.ecolsys.28.1.517>, 1997.

660 Shukla, P.R., Skea, J., Calvo Buendia, E., Masson-Delmotte, V., Pörtner, H.O., Roberts, D.C., Zhai, P., Slade, R.,
661 Connors, S., Van Diemen, R. and Ferrat, M.: Climate Change and Land: an IPCC special report on climate change,
662 desertification, land degradation, sustainable land management, food security, and greenhouse gas fluxes in terrestrial
663 ecosystems, IPCC., 874 pp., 2019.

664 [Czuchlewski, K.R. and Weissel, J.K., Synthetic Aperture Radar \(SAR\)-based mapping of wildfire burn severity and](#)
665 [recovery. In Proceedings. 2005 IEEE International Geoscience and Remote Sensing Symposium, 2005. IGARSS'05.](#)
666 [\(Vol. 1, pp. 4-pp\). IEEE. 10.1109/IGARSS.2005.1526102, July 2005.](#)

667 [Tanase, M.A., Santoro, M., De La Riva, J., Fernando, P. and Le Toan, T. Sensitivity of X-, C-, and L-band SAR](#)
668 [backscatter to burn severity in Mediterranean pine forests. IEEE Transactions on Geoscience and Remote Sensing,](#)
669 [48\(10\), pp.3663-3675. 10.1109/IGARSS52108.2023.10281609, 2010.](#)

670 [Peacock, A., Pinto, N. and Lou, Y. Burn Severity Mapping with L-band UAVSAR Observations Over Los Angeles’](#)
671 [Largest Wildfire. In IGARSS 2023-2023 IEEE International Geoscience and Remote Sensing Symposium \(pp. 3375-](#)
672 [3378\),10.1109/IGARSS52108.2023.10281609, July 2023.](#)

673 [Tanase, M., Santoro, M., de la Riva, J., Kasischke, E. and Korets, M.A. December. L-band SAR backscatter prospects](#)
674 [for burn severity estimation in boreal forests. In Proc. ESA Living Planet Symp. December 2010.](#)

675 [Bradley, C.M., Hanson, C.T. and DellaSala, D.A. Does increased forest protection correspond to higher fire severity](#)
676 [in frequent-fire forests of the western United States?. Ecosphere, 7\(10\), p.e01492, <https://doi.org/10.1002/ecs2.1492>,](#)
677 [2016](#)

678 [Xu, W., He, H.S., Hawbaker, T.J., Zhu, Z. and Henne, P.D. Estimating burn severity and carbon emissions from a](#)
679 [historic megafire in boreal forests of China. Science of the Total Environment, 716, p.136534,](#)
680 [https://doi.org/10.1016/j.scitotenv.2020.136534, 2020.](#)

681 [Meng, R., Wu, J., Zhao, F., Cook, B.D., Hanavan, R.P. and Serbin, S.P. Measuring short-term post-fire forest recovery](#)
682 [across a burn severity gradient in a mixed pine-oak forest using multi-sensor remote sensing techniques. Remote](#)
683 [Sensing of Environment, 210, pp.282-296, <https://doi.org/10.1016/j.rse.2018.03.019>, 2018.](#)

684 [Huerta, S., Marcos, E., Fernández-García, V. and Calvo, L., 2022. Short-term effects of burn severity on ecosystem](#)
685 [multifunctionality in the northwest Iberian Peninsula. Science of The Total Environment, 844, p.157193,](#)
686 [https://doi.org/10.1016/j.scitotenv.2022.157193, 2022.](#)

687 [Tanase, M., de la Riva, J., Santoro, M., Pérez-Cabello, F. and Kasischke, E. Sensitivity of SAR data to post-fire forest](#)
688 [regrowth in Mediterranean and boreal forests. Remote Sensing of Environment, 115\(8\), pp.2075-2085,](#)
689 [https://doi.org/10.1016/j.rse.2011.04.009, 2011](#)

690 [Addison, P. and Oommen, T. Utilizing satellite radar remote sensing for burn severity estimation. International journal](#)
691 [of applied earth observation and geoinformation, 73, pp.292-299, <https://doi.org/10.1016/j.jag.2018.07.002>, 2018](#)

692

693

694

695